PASJ: Publ. Astron. Soc. Japan **62**, 347–370, 2010 April 25

Subaru Near-Infrared Imaging of Herbig Ae Stars*

Misato FUKAGAWA,[1] Motohide TAMURA,[2,3] Yoichi ITOH,[4] Yumiko OASA,[5] Tomoyuki KUDO,[2] Saeko S. HAYASHI,[2,6] Eri KATO,[1] Takafumi OOTSUBO,[7] Yusuke ITOH,[1] Hiroshi SHIBAI,[1] and Masahiko HAYASHI[2,6]

[1]*Department of Earth and Space Science, Graduate School of Science, Osaka University, 1-1 Machikaneyama, Toyonaka, Osaka 560-0043*
misato@iral.ess.sci.osaka-u.ac.jp

[2]*National Astronomical Observatory of Japan, 2-21-1 Osawa, Mitaka, Tokyo 181-8588*

[3]*Department of Astronomical Science, The Graduate University for Advanced Studies (SOKENDAI), 2-21-1 Osawa, Mitaka, Tokyo 181-8588*

[4]*Graduate School of Science and Technology, Kobe University, 1-1 Rokkodai, Nada, Kobe 657-8501*

[5]*Department of Education, Saitama University, 255 Shimo-Okubo, Sakura, Saitama 338-8570*

[6]*Subaru Telescope, National Astronomical Observatory of Japan, 650 North A'ohoku Place, Hilo, HI 96720, USA*

[7]*Institute of Space and Astronautical Science, Japan Aerospace Exploration Agency, 3-1-1 Yoshinodai, Chuo, Sagamihara 252-5210*

(Received 2008 December 31; accepted 2010 January 22)

Abstract

We report results of H-band ($\lambda = 1.65\,\mu$m) imaging observations of young intermediate-mass stars using the Subaru 8.2-m Telescope with the adaptive optics AO36 and the infrared coronagraph CIAO. The targets consist of 16 Herbig Ae/Be stars (15 Herbig Ae stars and one Herbig Be star) and four additional main-sequence stars with infrared excesses. Five protoplanetary disks have been spatially resolved around the Herbig Ae stars with ages of 2–8 Myr. The resolved disks have outer radii of several 100 AU, and their surface brightnesses range from 10 mag arcsec^{-2} to 18 mag arcsec^{-2}. The images reveal various morphologies in optically thick disks: spiral arms around AB Aur, a banana-split structure with an outer arm for HD 142527, a compact circumprimary disk of HD 150193, a faint discontinuous ring around HD 163296, and an unstructured face-on disk of HD 169142. The detection of an optically thick disk in scattered light implies that it is vertically flared, and intercepts stellar light at least in the outer region where those images were obtained. However, the surface brightness distribution, the resolved structure, and other observational characteristics suggest that the disks are unlikely to be continuously flared young disks with small grains well mixed with gas. The detection rate and the disk brightness do not correlate with the stellar age and the disk mass, but there is a tendency that the brightest disks are still surrounded by long-lived envelopes (AB Aur, HD 100546, HD 142527). The significant diversity of the disk structure can be attributed to the multiplicity and the initial condition of the local star-forming environments. The detections of companion candidates around our targeted stars are also reported.

Key words: planetary systems: protoplanetary disk — stars: individual (HD 163296, HD 169142) — stars: pre-main sequence

1. Introduction

Circumstellar disks around pre-main-sequence (PMS) stars are believed to be birthplaces of planets, and thus an investigation of the disk properties is of primary importance to understand the process of planet building. The existence of a disk has long been predicted on the basis of spectral energy distributions (SEDs) (Adams et al. 1987, 1988). Most PMS stars have infrared (IR) excesses attributed to the reprocessing of stellar light by dust grains. IR studies initiated by the Infrared Astronomical Satellite (IRAS) confirmed that protoplanetary disks are ubiquitous for low-mass PMS stars (e.g., Cohen et al. 1989; Strom et al. 1989). Additional evidence suggestive of a disk has been known, such as jets and molecular outflow, which imply axisymmetry with a flat structure perpendicular to their axes (e.g., Mundt & Fried 1983). The centrosymmetric polarization pattern with aligned vectors close to the star indicates bipolar reflection nebula divided by the disk equatorial plane (e.g., Elsässer & Staude 1978; Bastien & Ménard 1988). Later observations have more directly revealed the disk nature. Rotating disks were detected with millimeter interferometry (e.g., Dutrey et al. 1994), silhouette disks were seen as extinction against the bright background (H II region) (O'Dell et al. 1993; McCaughrean & O'Dell 1996), and edge-on disks which naturally occult the central bright stars have been discovered (Burrows et al. 1996; Stapelfeldt et al. 1998).

Imaging observations enable us to study such properties as the surface brightness distribution, which reflects the dynamics of the disk material. High-spatial-resolution required for the disk imaging can be obtained in optical and near-infrared (NIR) using the Hubble Space Telescope (HST), or the combination of a large aperture telescope and adaptive optics. While edge-on systems are relatively easier to detect, and allow better

* Based on data collected at the Subaru Telescope, which is operated by the National Astronomical Observatory of Japan.

Table 1. Observed targets.

Source	Spectrum	References*	d (pc)	Reference†	A_V	$\tau = L_{\rm IR}/L_*$	Age (Myr)
AB Aur	A1	1	144	1	0.50	0.43 ± 0.03	3
MWC 480	A5	2	170	13	0.096	0.44 ± 0.03	5
HD 34282	A3	4	350	3	0.16	0.58 ± 0.05	ZAMS‡
HD 139614	A7	3	140	6	0.093	0.39 ± 0.02	> 10
HD 142527	F6	8	140	6	0.37	1.09 ± 0.04	2
HD 144432	A9	2	145	8	0.16	0.35 ± 0.03	4
HD 149914	B9.5	6	165	4	0.66	2.1×10^{-3}	$\lesssim 1$
HD 150193	A2	2	150	1	1.5	0.29 ± 0.03	6
KK Oph	A8	2	160	12	2.5	0.69 ± 0.04	5
HD 163296	A1	2	122	1	0.16	0.36 ± 0.03	4
HD 169142	A5	3	145	7	0.31	0.27 ± 0.03	8
VV Ser	B6/A0	1/2	310	11	3.0	1.1 ± 0.1	5
HD 176386	B9	5	140	1	0.62	< 0.12	2
HD 179218	A0	2	240	2	0.53	0.23 ± 0.02	1
HD 190073	A2	2	> 290	2	0.19	0.30 ± 0.03	1
HD 200775	B3	1	430	1	1.9	0.11 ± 0.03	< 0.1
HD 131885	A0	6	121	10	0.12	$(4.7 \pm 0.4) \times 10^{-4}$	
HD 184761	A8	9	65	5	0.00	$(1.0 \pm 0.5) \times 10^{-2}$	ZAMS§
HD 191089	F5	7	54	9	0.031	$(1.6 \pm 0.2) \times 10^{-3}$	$\lesssim 100$‖
HD 218396	A5	10	39	14	0.34	$(2.0 \pm 0.4) \times 10^{-4}$	30‖

* 1. Hernández et al. (2004), 2. Mora et al. (2001), 3. Dunkin, Barlow, and Ryans (1997a), 4. Merín et al. (2004), 5. Bibo, Thé, and Dawanas (1992), 6. Houk and Smith-Moore (1998), 7. Houk (1982), 8. Houk (1978), 9. Miroshnichenko et al. (1999), 10. Skiff (2003).

† 1. van den Ancker et al. (1997), 2. van den Ancker, de Winter, and Tjin A Djie (1998), 3. Merín et al. (2004), 4. Sartori, Lépine, and Dias (2003), 5. Miroshnichenko et al. (1999), 6. de Zeeuw et al. (1999), 7. Sylvester et al. (1996), 8. Pérez et al. (2004), 9. Zuckerman and Song (2004), 10. Sylvester, Dunkin, and Barlow (2001), 11. de Lara, Chavarria-K, and López-Molina (1991), 12. Leinert et al. (2004), 13. Simon, Dutrey, and Guilloteau (2001), 14. van Leeuwen (2007).

‡ 6.4 Myr was derived in Merín et al. (2004) using the appropriate metallicity.

§ Miroshnichenko et al. (1999).

‖ Zuckerman and Song (2004).

constraints on the vertical thickness, face-on ones are favorable to obtain the radial structure and the overall morphology of a disk. Coronagraphy is indispensable to improve the detectability of the scattered emission from such a disk buried in the bright stellar halo. Several disks around T Tauri and Herbig Ae stars have been resolved so far, mostly by the HST coronagraphs (e.g., Weinberger et al. 1999; Grady et al. 2005b). However, we are far from understanding the general properties of the disks due to poor statistics. Moreover, once a disk is spatially resolved, follow-up studies at multi-wavelength and multi-epoch can enhance our knowledge of it, and allow a detailed comparison with theoretical work on planet formation. It is hence important to sustain the effort to obtain resolved disk images.

Herbig Ae/Be stars are PMS stars covering a mass range of 2–10 $M_\odot$ (Herbig 1960). There had been arguments as to the disk existence for Herbig Ae/Bes. A spherical envelope, a circumstellar disk, or a combination of both, all provided acceptable fits to the SEDs (Hartmann et al. 1993; Pezzuto et al. 1997; Chiang et al. 2001; Miroshnichenko et al. 1999). Flared disk models with the inclusion of a puff-up inner rim were successful to reproduce a strong NIR excess (Natta et al. 2001; Dullemond et al. 2001) without the need of other components, but the possibility of an envelope-like halo is not completely excluded. Observationally, disks do exist around Herbig Ae stars (from B5 to F) with many similarities to those around T Tauri stars, whereas disks around higher-mass stars apparently show different characteristics (Vink et al. 2002; Eisner et al. 2004; Alonso-Albi et al. 2009). The circumstellar disks around nearby Herbig Ae stars have been resolved at (sub-)millimeter wavelengths, in both dust continuum and CO lines with almost Keplerian rotation (Mannings & Sargent 1997, 2000; Piétu et al. 2003). In scattered light, recent high-resolution imaging studies with HST have revealed disks around Herbig Ae stars with several million years of age (e.g., Grady et al. 2005b). Therefore, Herbig Ae stars are generally recognized to be precursors of early type Vega-like stars with debris disks, such as β Pictoris. Their circumstellar environments represent early stages of *possible* planet formation around intermediate-mass stars.

The target stars are shown in section 2. In sections 3 and 4, we describe the Subaru observations and reduction procedures. Each resolved disk and non-detections are presented in section 5.

2. Targets

The observed targets consist of 16 Herbig Ae/Be stars and additional 4 Vega-like stars with intermediate-masses (table 1). Their distances were measured by Hipparcos for most of the targets (van den Ancker et al. 1997, 1998; Zuckerman & Song 2004). The photometrically derived distances were taken

from the literature for stars located beyond 200 pc without Hipparcos measurements, and those with large uncertainties in the Hipparcos distances. If such a star belongs to any moving group, the cluster distance may give a reasonable value. We assumed the mean distance of Upper Scorpius Lupus (de Zeeuw et al. 1999; Teixeira et al. 2000) for HD 139614 and HD 142527. The A_V was calculated using $E(B-V)$ from Bessel et al. (1998) and the ratio of total-to-selective extinction, $R_V = A_V/E(B-V)$, of 5.0 which is preferred for most Herbig Ae/Be stars (Hernández et al. 2004). The fractional IR luminosities ($L_{\rm IR}/L_*$) and ages are estimated from the SEDs, as described in section 5.

2.1. Herbig Ae/Be Stars

The stars best suited to coronagraphic imaging are nearby, minimally extincted, and lack obscuring nebulosity such as molecular cloud material or circumstellar envelopes. Our targets, except for HD 200775, are not deeply embedded in the molecular clouds and relatively *isolated*. The typical IR excess is on an order of 10^{-1} ($L_{\rm IR}/L_* \sim 10^{-1}$), implying that the disk should be optically thick (e.g., Adams et al. 1987; Chiang & Goldreich 1997). The optical thickness has also been inferred by the imaging of disks around such stars in scattered light (e.g., Krist et al. 2000). Most sources are nearby ($d < 200$ pc), while distant sources are also included if the high possibility of resolving disks is suggested by the millimeter or speckle observations (HD 34282, VV Ser). Binaries are not excluded.

2.2. Vega-Like Stars

Several disks have been successfully imaged in NIR around relatively young, rich excess stars, like β Pictoris, HR 4796A, HD 32297, HD 181327, and HD 15115 (Mouillet et al. 1997; Schneider et al. 1999, 2005, 2006; Kalas et al. 2007). In fact, some are even brighter than the majority of disks around Herbig Ae stars. Vega-like stars with large IR excesses ($L_{\rm IR}/L_* \sim 10^{-3}$) found by IRAS were chosen, since they would have a high chance of being detected. HD 131885, HD 184761, and HD 191089 have additional evidence of abundant dust and/or youth of the system, such as a large polarization (Bhatt & Manoj 2000) and young age determined by more than one method (Zuckerman & Song 2004). Because the sources are located within 150 pc, the disk structure with the typical size of 100 AU can be resolved. HD 218396 was selected based on its proximity ($d = 39.4$ pc: van Leeuwen 2007), although with its moderate infrared excess, $L_{\rm IR}/L_* = 2.0 \times 10^{-4}$.

3. Observations

3.1. Subaru/CIAO

Imaging observations were conducted with the coronagraphic camera CIAO (Coronagraphic Imager with Adaptive Optics: Tamura et al. 2000) mounted on the Subaru 8.2-m Telescope (Iye et al. 2004) from 2002 July to 2004 June. CIAO is equipped with a 1024×1024 InSb ALADDIN II array, and is capable of observations in NIR, 1–5 μm. The array was replaced in 2003 by a new one, giving a slightly higher sensitivity. The images were obtained in the H band for all targets. Additional K-band imaging was carried out for HD 142527 and AB Aur, and J-band images were also taken for AB Aur. The medium-resolution mode (21 mas pixel^{-1}) was used rather than the high resolution one (11 mas pixel^{-1}) in order to obtain higher sensitivity for extended emission. The pixel scale was 21.25 ± 0.03 mas pixel^{-1} and 21.33 ± 0.02 mas pixel^{-1}, before or after the array replacement, respectively (Itoh et al. 2002, 2005).

The classical Lyot coronagraph for CIAO consists of two optical components, an occulting mask at the focal plane and a Lyot stop at the pupil plane (Lyot 1939). The occulting mask is made of a chrome spot evaporated on a sapphire substrate. The $\sim 1\%$ (0.1%–2%) transmission of the chrome film enables us to detect the peak of a masked star, and thus to measure the stellar position with 0.3 pixel accuracy. We used a circular Lyot stop, which blocked out the outer 20% of the pupil diameter without spider masking and pupil apodization. The coronagraph works ideally when most of the incident light is occulted. A low-order AO system like the Subaru AO with 36 elements (Takami et al. 2004), however, has not yet provided such high performance. The typical Strehl ratio obtained with the Subaru AO36 in the H band is $\lesssim 0.2$ (Takami et al. 2004; Itoh et al. 2002). However, the coronagraphic capability of CIAO improves the observational efficiency, especially for bright sources, like Herbig Ae/Be stars. The occulting mask is quite useful to avoid saturation, which allows longer exposures, and reducing stellar light in the optical system.

A wide range of the mask size was provided for CIAO, from $0\farcs1$ to $4\farcs0$ in diameter. A smaller size was favorable to probe the inner region, but it required a shorter exposure time, and thus a lower observation efficiency, since the read-out noise became dominant. We used a $\sim 0\farcs5$ mask at first in 2002, but based on experience of these observations, a $1\farcs0$ mask was employed with longer exposures for deeper imaging to detect fainter disks in 2004. The AO guide star was the target, itself, since the targeted stars had little nebulosities, and were bright enough in the R band where the AO monitors atmospheric turbulence.

3.2. PSF Reference Stars

The most critical post-process to reveal faint circumstellar material is subtraction of the Point Spread Function (PSF). It is important to obtain a stellar PSF whose size and shape are the same as those of the target star. If there is a mismatch in PSFs, an artificial disk easily appears, or a real one disappears. First, the reference star should have a similar brightness in the R band where the AO works. Since our targets were too bright ($R < 10$ mag) for the AO, except for VV Ser, the neutral density filters in the AO module were used, and the R magnitudes should be matched while taking into account extinction by the filters. Another important criterion is that there is no nearby source that affects the PSF. In addition, the PSF star should be located close to the star (within $\sim 10°$). The NIR color could be another factor to determine the PSF, but we put more weight on having a similar R brightness, and did not attempt to select reference stars with similar NIR colors. We describe the color effect in subsection 5.2.

The observed sources are listed in table 2; $R_{\rm obs}$ in column 4 is the incident light to the wavefront sensor (avalanche photodiode modules) used to measure the atmospheric turbulence.

Table 2. Observation log.*

	Source	R (mag)	$R_{\rm obs}$ (mag)	H (mag)	Δr (°)	Mask	Each exp. (s)	Total exp. (min)	Date
object	HD 144432	8.0	10.5	6.5		0.″5	3	5.7	2002 Jul 17
ref.	HD 144176	7.8	10.2	7.2	0.8	0.″5	5	9.5	
object	HD 150193	8.6	10.0	6.2		0.″5	1	12.8	2002 Jul 17
ref.	HD 150734	7.9	10.6	7.0	1.2	0.″5	5	12.0	
object	KK Oph	10.9	11.8	7.2		0.″5	3	23.8	2002 Jul 18
ref.	HD 154625	9.4	11.9	8.4	1.0	0.″5	5	19.3	
object	HD 169142	8.2	10.4	6.9		0.″5	3	34.0	2002 Jul 18
ref.	HD 169919	8.3	10.4	7.0	1.7	0.″5	3	18.8	
object	HD 190073	7.8	10.5	6.6		0.″5	3	12.6	2002 Jul 17
ref.	HD 189510	7.7	10.8	7.8	1.7	0.″5	5	13.3	
object	HD 200775	7.3	11.0	5.5		0.″5	1	21.0	2002 Jul 18
ref.	SAO 19214	6.8	10.9	6.5	1.5	0.″5	2	20.0	
object	HD 218396	6.0	10.6	5.3		0.″5	1	21.9	2002 Jul 18
ref.	HD 218172	7.3	10.9	5.9	1.0	0.″5	1	16.5	
object	MWC 480	7.6	10.1	6.3		0.″5	2	8.0	2002 Nov 24
ref.	SAO 76547	8.6	10.0	8.2	10.5	0.″5	10	17.0	
object	HD 34282	9.7	10.9	8.5		0.″8	10	17.5	2003 Jan 5
ref.	HD 34737	8.7	11.1	8.7	0.8	0.″8	10	18.0	
object	AB Aur†	7.0	10.8	5.1		0.″6	0.33, 1	18.6	2004 Jan 8
ref.	SAO 57754	6.2	10.6	5.2	8.1	0.″6	1	5.2	
object	HD 139614	8.1	10.4	7.3		1.″0	10	18.0	2004 Jun 4
ref.	HD 138255	8.0	10.4	7.2	1.8	1.″0	10	11.2	
object	HD 139614‡					1.″5	20	2	2008 May 23
object	HD 163296	6.8	10.5	5.5		1.″0	3	25.0	2004 Jun 4
ref.	HD 156365	6.2	10.6	5.2	9.0	1.″0	3	20.0	
object	HD 191089	6.9	10.8	6.1		1.″0	5	19.0	2004 Jun 4
ref.	HD 197746	6.8	10.6	6.0	8.4	1.″0	5	14.0	
object	HD 191089	6.9	10.8	6.1		1.″0	5	15	2004 Jun 6
ref.	HD 197746	6.8	10.6	6.0	8.4	1.″0	5	13	
object	HD 131885	6.9	10.7	6.7		1.″0	5	27.0	2004 Jun 5
ref.	HD 131992	6.9	10.6	6.4	0.9	1.″0	5	16.0	
object	HD 142527	6.7	10.2	5.7		1.″0	5	22.7	2004 Jun 5
ref.	HD 137785	6.3	10.0	5.6	6.4	1.″0	5	11.0	
ref.	HD 145191	5.7	10.2	5.3	3.0	1.″0	5	11.0	
object	HD 142527‡					1.″0	3	0.5	2008 May 24
object	VV Ser	11.0	11.0	7.5		1.″0	10	26.0	2004 Jun 5
ref.	HD 166992	7.3	11.1	7.1	4.3	1.″0	10	16.0	
object	HD 184761	6.6	10.3	6.1		1.″0	10	22.0	2004 Jun 5
ref.	HD 184151	6.6	10.3	5.7	1.8	1.″0	5	8.5	
object	HD 179218	7.3	11.0	6.6		1.″0	10	26.0	2004 Jun 5
ref.	HD 177305	7.3	11.0	6.2	2.3	1.″0	10	20.0	
object	HD 149914	6.6	10.3	5.8		1.″0	3	19.0	2004 Jun 6
ref.	HD 144134	6.5	10.3	5.7	7.9	1.″0	3	14.6	
object	HD 176386	7.3	11.0	6.8		1.″0	5	20.0	2004 Jun 6
ref.	HD 189387	7.4	11.2	6.5	16.1	1.″0	5	13.0	

* The detector array was replaced in the fall of 2003 by a new one with a slightly better sensitivity, as noted with the double line. R magnitudes are taken from the USNO-B1.0 catalog (Monet et al. 2003), and H magnitudes of reference stars are from the 2MASS All-Sky Catalog of Point Sources. For H magnitudes of target stars, 2MASS photometry was adopted when other measurements could not be found in literature.

† The J- and K-band short exposures were also taken on the same night.

‡ The J- and K-band observations were also carried out on 2008 July 12.

When neutral-density filters were inserted, $R_{\rm obs}$ was fainter than the original R magnitude. In column 6, the separation between the target source and the PSF reference star is shown. We also indicate the diameter of the occulting mask in column 7, the exposure time per one read-out in column 8, and the total exposure time in column 9. Several read-outs were coadded into one frame when the seeing condition was stable in order to reduce the observational overhead.

3.3. Observing Procedure

We first adjusted the AO configuration (voltage of the vibration mirror, the gain of the deformable mirror, the radius of iris etc.) for obtaining the best AO performance under the given sky condition, then took exposures of a PSF reference star first, a target source next, and again observed a PSF reference star. Additional exposures were obtained when Vega-like stars expected to have fainter disks were observed, or when the resolved structure was found through a real-time quick reduction. In order to avoid temporal variation of a PSF, the interval between a PSF and a target star was set to be within 45 min. Since the stellar position against the center of the occulting mask gradually moved, re-centering was frequently needed with the AO tip-tilt mirror. This can be caused by a difference in the atmospheric refraction between NIR and optical in which AO works. Dithering by $\sim 1''$ was performed once during the observations of a science target by moving the mask and stellar positions while keeping the AO loop closed. The observing time was 1.5–2.0 hr in each sequence, and the total exposure time for one target was 10–30 min after selecting only usable data frames, which strongly depends on the seeing conditions. The seeing size was $0\farcs5$–$1''$ in optical, and the overall seeing condition (size and stability) was better in 2004 June than in 2002 July, resulting in better detection limits in 2004 (see subsection 5.2). The sky was covered by cirrus on July 17 in 2002, by clouds for MWC 480, but clear for other nights.

We note that unocculted photometry for science targets was not carried out, and past measurements by 2MASS or Malfait, Bogaert, and Waelkens (1998) were used for the later discussion, although there is a possibility of variability in IR excess emission (Sitko et al. 2008). To roughly check whether this assumption would have a large impact on our discussion about the disk luminosity in scattered light (subsection 5.5), photometry of the masked star was attemped. It produced a 0.1–0.3 mag uncertainty for a $1''$ mask, and worse ($\lesssim 0.5$ mag) for a $0\farcs5$ mask. A comparison with the masked PSF reference star suggests that within these uncertainties, there are no noticeable differences from the 2MASS magnitudes for those sources with resolved disks, AB Aur, HD 142527, HD 163296, and HD 169142. For HD 150193, photometry with similar accuracy was difficult due to the PSF variation and the lower signal-to-noise ratio (S/N) of the transmitted light.

3.4. Imaging at the Second Epoch for Companion Candidates

HD 142527 and HD 139614 were also imaged in 2008 to verify if companion candidates found in 2004 were comoving with them. HD 142527 was observed with CIAO on May 24 and July 12. In the May observations, 10 data frames were obtained with each exposure time of 3 s in the H band. J- and K-band images were obtained in July, with 22 frames of 3 s exposure in the J band, and with 30 frames of 2 s exposure in the K band. We used the AO36 and an occulting mask of $1\farcs0$ in diameter.

HD 139614 was also observed on May 23 and July 12. H images were taken in May with a $1\farcs5$ mask and the AO. The exposure time was 20 s for each frame, and a total of 6 frames were obtained. J- and K-band imaging was conducted on July 12. The seeing condition was much worse in July ($> 1''$), and hence more exposures were needed for the photometry of a faint companion candidate. We obtained 24 and 18 frames with 20 s exposure time in the J and K bands, respectively. Skies were clear on these three nights. They were observed under photometric conditions.

4. Data Reduction

The obtained data frames were calibrated in a standard manner using the Image Reduction and Analysis Facility (IRAF): dark subtraction, flat-fielding, sky subtraction, and badpixel substitution. The dark frames were obtained either or both before/after each observing night. We used dome-flats or twilight-flats for flat-fielding for the data taken in 2002 or after 2003, respectively. The sky was estimated as a median value measured where no emission was found.

PSF-subtraction is indispensable in order to reveal faint cricumstellar material buried in the bright halo of the central star. At the same time, it requires a careful treatment so as not to generate an artificial circumstellar structure in the three reduction steps: frame selection, matching the stellar positions, and scaling of the reference PSF.

First, all frames were shifted to have the same stellar positions. The position of an occulted star could be measured thanks to transmission ($\sim 1\%$) of the coronagraphic masks. Centroid measurements with a positional accuracy of ~ 0.3 pixel (6.39 mas) were performed, and the images were shifted by bilinear interpolarion.

The observed PSFs were usually affected by a short time scale variation of the seeing. Therefore, it was needed to examine each PSF and to avoid including data frames with larger or more elongated PSFs compared with others. Since the star was occulted by the coronagraphic mask, the FWHM was not accurately measured. We then employed the intensity ratio between the peak and the halo as a measure of the PSF size. The intensity of the halo was measured at $r = 1\farcs5$ or $1\farcs0$, depending on the S/N at the outer skirts of the PSF. The validity of this measure was confirmed by comparing the intensity ratio of the target and the FWHMs of the unmasked point sources when they existed in the field of view (FOV, $22''$). A good correlation was found between them, and the intensity ratio was even better than the FWHM for identifying both the shape and the size, which were verified by the smaller PSF-subtraction residuals produced when frame matching was performed based on the intensity ratio. We selected the target frames so that the dispersion of the peak/halo brightness ratio would be within 20%–30%. Because the seeing was stable on 2004 January 8 and 2004 June 4, most data frames obtained on those nights were usable. However, the seeing variation was significant on the other nights, and $\sim 50\%$ of the obtained

frames were not suited for PSF-subtraction, and were thus discarded. For the reference PSF stars, appropriate frames were chosen in the same manner as for the science target, so that the PSF sizes would be similar to those of the targeted star. Since the reference stars were not always much brighter than the science targets, reference PSF frames taken at close times were average-combined to increase the S/N after matching the spider directions.

The reference PSFs were subtracted from each target image. Flux scaling of the reference PSF was made based on the halo intensity at $r = 1\farcs5$ or $1\farcs0$. This scaling was not always successful, and obviously unreasonable when the target had a bright circumstellar structure. It was also attempted to match the peak intensities or to scale the PSF based on the H-band brightness ratio between the object and the reference stars. Nevertheless, fine adjustment of the scaling and the registration was needed to minimize the residuals for each subtracted image. The subtracted frames were finally combined. The subtraction procedure caused a flux uncertainty of 10%–25% in the final image, depending on the degree of the variation of PSFs or the mismatch between the PSFs of the target and the reference star.

If there was any point source whose halo contaminates the PSF-subtracted image for the targeted source, additional subtraction was required from the nearby point source. In that case, a binary PSF was created using the duplicated PSF that was shifted, scaled based on the brightness ratio to the target star, and combined with the primary PSF. PSF subtraction for an unmasked nearby star using the masked PSF was apparently acceptable for our observations. The PSF shape should be varied depending on the mask size as well as on the AO performance, but the use of a small mask and the imperfection of the AO correction resulted in poor halo suppression. Therefore, subtraction of the masked binary PSF was carried out in order to examine the disk around the target source, but we do not discuss the circumstellar emission around the nearby point source conservatively.

Even when the residual emission is detected around the star after the PSF-subtraction, there is a possibility that the emission is an artifact. Faint circular distribution might be generated due to incorrect scaling for the PSF, or bright but compact ($r \lesssim 2 \times$ mask radius) emission is difficult to be distinguished from the PSF-residual. The temporal stability of the emission was examined to check if it was real. We also concluded that the emission was likely to be attributed to a circumstellar disk when at least one of the following conditions was satisfied: (1) the emission was extended ($r \gtrsim 5 \times$ mask radius), (2) the same/similar results were obtained with observations at different epochs, (3) there was an additional evidence of its existence, such as optical imagery or polarization maps.

Resolved disk images around HD 163296 and HD 169142 obtained with Subaru are presented for the first time in later subsections, while details for other resolved disks have been reported in previous publications (Fukagawa et al. 2003, 2004, 2006). We describe the observations and reduction procedures for HD 163296 and HD 169142 below.

4.1. HD 163296

HD 163296 was occulted by a mask of $1\farcs0$ diameter. Two exposures of 3 s were coadded into one data frame and 250 frames were obtained. The total integration time was then 25 min. We observed the PSF reference star HD 156365 just before and after observing HD 163296. In the same way as HD 163296, two exposures of 3 s were coadded into one frame. The total exposure time of HD 156365 was 11 min and 9 min, before and after observing HD 163296, respectively. Although the seeing was stable that night, a slight mismatch of the PSF shape was seen between the object and the PSF reference in part of the frames. Such frames were discarded, and the remaining 169 PSF-subtracted frames (= 16.9 min) were combined. A spatial resolution of $0\farcs094$ (= 11.5 AU) was achieved, estimated from the FWHMs of the field point sources.

4.2. HD 169142

An FWHM of $0\farcs12$ was achieved, and an occulting mask with a diameter of $0\farcs5$ was used for HD 169142. The five exposures of 3 s were coadded into one data frame, and the total integration time for HD 169142 was 34 min. Among them, 60 frames corresponding to 15 min integration were chosen for PSF-subtraction. For the PSF star HD 169919, the integration time per frame was the same as that for HD 169142, and the total integration time was 19 min. PSF-subtraction was performed in two different ways. First, subtraction was carried out using the PSF for the observed reference star. The resulting image suggested extended material out to $r \sim 1\farcs4$. However, there was a noticeable difference in the PSF shape between HD 169142 and the reference star, which could affect the disk structure in the case of a faint face-on disk like observed around HD 169142. Therefore, we also attempted PSF-subtraction using the PSF of another point source in the same FOV. There was only one source with sufficient brightness in the small FOV of CIAO, located with the separation of $9\farcs38 \pm 0\farcs01$ and a position angle (P.A.) of $-135\fdg5 \pm 0\fdg6$ from HD 169142. This object is not an ideal reference, since it is a T Tauri binary separated by $0\farcs13$ (2M 1824 AB: Grady et al. 2007), and may cause an over-subtraction or elongated residual emission. However, no clear sign of disks around the binary has been suggested (Raman et al. 2006), and the difference of the FWHM from other field stars was within the degree of temporal variation during observations. To extract the PSF of 2M 1824 AB, a rough subtraction was first performed using an image of HD 169919 in order to remove any contribution from the bright halo of HD 169142. 2M 1824 AB is about 6.6-times fainter than HD 169142, and 30 frames were combined into one image to improve the S/N. Given the small disk size, the obtained S/N for each PSF was acceptable, where S/N > 10 at $r < 1\farcs9$. The combined PSF was subtracted from each original frame after being shifted to the position of HD 169142. In most frames, the resultant disk images appeared to be more circular than when using images of HD 169919, and no disk elongation perpendicular to the binary position angle was found. A difference from the results with HD 169919 was seen in the southern part of the disk, where there was an over-subtraction due to the elongation of HD 169919, but the outer radius is consistent with each other.

5. Results and Discussion

5.1. Resolved Disks

Circumstellar structures were detected around AB Aur, HD 142527, HD 150193, HD 169142, and HD 163296. Images of AB Aur, HD 142527, and HD 150193 have already been published (Fukagawa et al. 2004, 2006, 2003), and thus we just describe those objects briefly below.

5.1.1. AB Aur

What is remarkable for this object is a spiral structure clearly seen in the outer disk (Fukagawa et al. 2004). The disk structure has influence on the evolutionary process invoking planet formation; thus, of interest is such a morphology with a significant deviation from the standard view of a protoplanetary disk with smoothed radial density distributions. Oppenheimer et al. (2008) and Perrin et al. (2009) conducted high-resolution imaging polarimetry in NIR to get closer to the star, and thus obtaining disk images from $r = 0\farcs3$ with a *polarization* depleted zone northwest at around 100 AU.

We also observed AB Aur in the J and K bands, although with a much lower S/N than that in the H band. The brightness ratio of the scattered flux to the total flux was calculated for the radial range of 120 AU $\leq r \leq$ 300 AU, where S/N ≥ 2, giving $F_{\rm disk}/F_{\rm total} = (1.4 \pm 0.3) \times 10^{-2}$ in the J band. The ratio measured in the same region was $F_{\rm disk}/F_{\rm total} = (0.9 \pm 0.2) \times 10^{-2}$ and $(1.0 \pm 0.2) \times 10^{-2}$ in the H and K bands, respectively, indicating that the disk is marginally blue in $J - H$, but neutral in $H - K$.

5.1.2. HD 142527

The H- and K-band images reveal a peculiar structure with an inner hole and an outer arm (Fukagawa et al. 2006). The inner cavity detected in scattered light was also confirmed in mid-infrared (Fujiwara et al. 2006) and with a submillimeter dust continuum (Ohashi et al. 2010), suggesting that the cavity is devoid of dusty material. The cavity is likely to be a wide gap, since HD 142527 has a substantial NIR excess. The observed gap may indicate the presence of unseen companions.

5.1.3. HD 150193

HD 150193 was observed in 2002 July, since the existence of circumstellar material had been suspected by our observations in 2001, but under a terrible seeing variation. Although the seeing was not very stable also in the second run in 2002, a similar circumstellar emission in both observing runs led us to conclude that the disk was likely to be resolved (Fukagawa et al. 2003). The disk is not very large (190 AU), and shows asymmetry that might be due to the presence of a companion, classified as a Weak-line T Tauri star by Carmona, van den Ancker, and Henning (2007). In general, a star with a companion separated at the typical disk radius ($\sim$ 100 AU) would have a truncated disk, suggesting a low detection rate of the disk with direct imaging. The projected separation between HD 150193 A and B is 165 AU, but the real separation between them is unknown, and might be much larger. For a relatively compact disk, like the one observed, the detectability and the disk property, such as the disk shape and the brightness are easy to be affected by the quality of the PSF. Further confirmation would be important for this object.

5.1.4. HD 163296

HD 163296 (A1Ve: Mora et al. 2001) is one of the well-studied Herbig Ae stars, located at $d = 122^{+17}_{-13}$ pc (van den Ancker et al. 1997). Its age and stellar mass are estimated to be 4–6 Myr and $2.3 \pm 0.1\,M_{\odot}$, respectively. The dust continuum emission was resolved by millimeter interferometry with its size of 200 AU in radius; the CO Keplerian disk was also detected out to 540 AU (Isella et al. 2007). The inclination was estimated to be $i = 46^{\circ} \pm 4^{\circ}$ with the P.A. of $128^{\circ} \pm 4^{\circ}$ (Isella et al. 2007). In the optical region, a faint, but extended, disk has been observed with HST/STIS (Grady et al. 2000), with the outer radius of $\sim$450 AU. The high resolution allowed us to trace remarkable features as a dark lane at $r = 325$ AU and bright ansae beyond it. The optical image and the FUV spectra with HST/STIS showed Herbig–Haro flow with blue-shifted emission toward the southeast and red-shifted toward the northeast with the P.A. $= 45\fdg15$ (Devine et al. 2000), which is consistent with the direction of the disk polar axis. The shallow wavelength dependence of millimeter fluxes and the IR spectra require a population of large, millimeter to centimeter sized grains (Bouwman et al. 2000; van den Ancker et al. 2000).

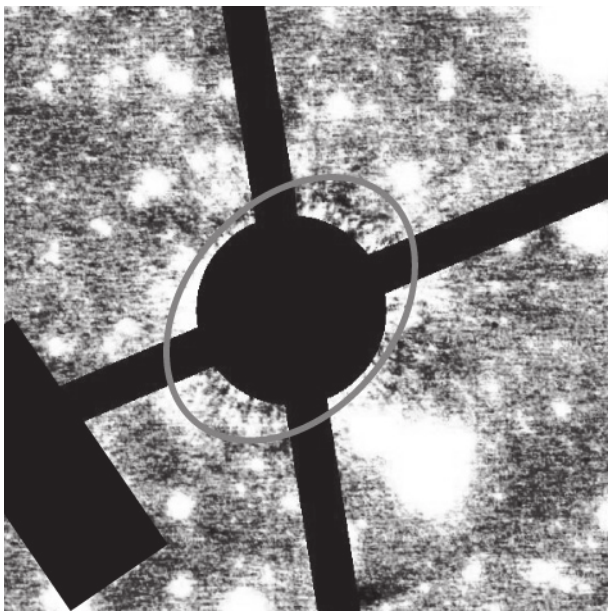

Fig. 1. H-band image of a circumstellar disk around HD 163296 obtained in 2004. The software mask occults the central region $r \leq 1\farcs9$ where the PSF residuals are dominant. The spider pattern and the ghost images at the bottom left corner are also software-masked. The image is overlaid with the ellipse having the semi-major axis of $3\farcs0$ and P.A. $= 140^{\circ}$. North is up and east is to the left.

In our observations, faint discontinuous ring-like emission around HD 163296 was detected out to $r = 3\farcs6$ (= 440 AU) (figure 1). The large outer radius and the inner depletion make it easier to identify the disk regardless of the faintness. Although the S/N is low (S/N = 2 at the peak intensity), elliptic emission clearly appears as in an optical image taken by HST/STIS (Grady et al. 2000). Assuming that the circumstellar emission is circular, the position and inclination angles were measured by fitting an ellipse, resulting in P.A. $\sim 140^{\circ}$ and $i \sim 45^{\circ}$, respectively. The spatial extent and the elliptical geometry are in agreement with those observed at millimeter wavelengths as well as that imaged in the optical band. The

emission detected in the H band can thus be interpreted as light scattered by dust grains residing in the disk.

The disk morphology roughly coincides with that detected in the optical region by Grady et al. (2000). The PSF subtraction residual was dominant in the inner most part ($r < 1\farcs9$). Beyond $r = 1\farcs9$, there is a dark annulus, which can be recognized in our image in the direction of the semi-major axis, northwest and southeast of the star. Outside the dark lane, there are pieces of the annulus. In the southeast, the emission begins at $r = 2\farcs4$ and ends at $r = 3\farcs3$ with an almost flat brightness distribution in this radial range. In the northwest, emission was found in $r = 2\farcs6$–$3\farcs5$. The surface brightness of the ring was measured in the southeastern and northwestern parts of the annulus, resulting in $H = 17.5 \pm 0.3\,\mathrm{mag\,arcsec^{-2}}$. This is about 10-times fainter than the disk around AB Aur measured at the same radius, and even fainter than the peak brightness of the optically thin disk around HD 141569 A (Augereau et al. 1999). The total scattered flux is difficult to be derived due to a lack of sensitivity and contamination from the background stars. In addition, the faint annulus is easy to be split up by a mismatch of the PSF shape of the reference star. We thus assumed an elliptic annulus with a uniform brightness distribution of $17.5\,\mathrm{mag\,arcsec^{-2}}$ in $r = 2\farcs4$–$3\farcs5$ in order to estimate the upper limit of the disk flux in scattered light. The disk flux normalized by the total flux is 2×10^{-4}, which turns out to be smaller than that for β Pic. Note that we here discuss only the outer and upper parts of the optically thick disk.

The dark region just outside of the coronagraphic mask suggests two possibilities about the true disk morphology. A straightforward interpretation is that the inner portion of the disk is cleared out, which involves an evolutionary process, like dust aggregation or gap opening by unseen planets. It is expected that even in that case the hot disk at the very innermost would still exist, since the observed bipolar jets imply that the inner accretion has not yet been terminated. In addition, HD 163296 has sufficient NIR excess, and there is no noticeable dip in the IR SED. Moreover, Wisniewski et al. (2008) did not detect a dark lane in their observations in 2003 with the HST/ACS. Therefore, dust coagulation and the settlement could have been occurred, but the disk might not yet be evacuated.

Of remarkable interest is that the surface brightness in scattered light changes with time (Wisniewski et al. 2008), while the star itself is photometrically more stable. Wisniewski et al. (2008) reported that the disk was in a relatively faint state in 2004. Although the wavelength is different, our results with the faint structure would be consistent with their results, because the southeast ansa brightly appears in our and their images. In order to understand the mechanism of the variation, the inner-disk property could be a key. Sitko et al. (2008) has revealed a significant ($\sim$20%) increase in emitted flux at around 3 μm in 2002. They suggested that this NIR variation indicates a structural change in the dust sublimation zone, possibly inflating the inner wall of the dusty disk. Changes in the scale height of the inner wall could cause variable shadowing, resulting in variable illumination of the outer region. Observations to derive the timescale of the variation and the correlation between the inner and outer disks are crucially important.

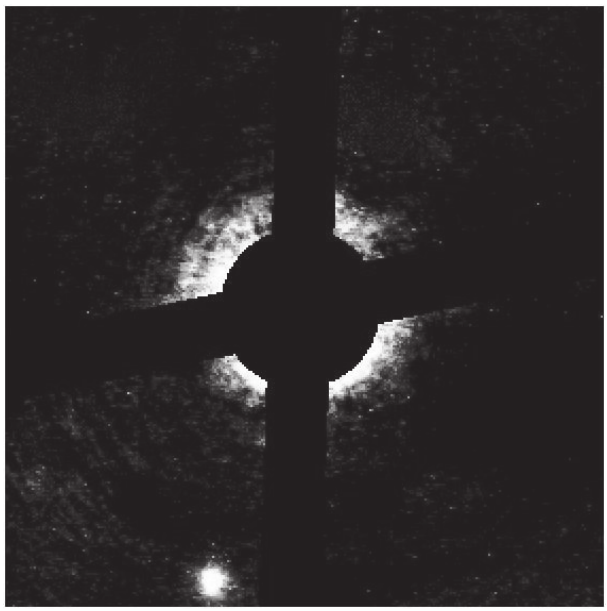

Fig. 2. H-band image of a circumstellar disk around HD 169142. The PSF-subtraction was performed using the PSF of the source at $9\farcs4$ from HD 169142. The inner region $r \leq 0\farcs8$ is software-masked where the PSF-subtraction error affects the disk image. The secondary spider pattern is also masked numerically. The image is linearly displayed with the intensity range from 1σ to 20σ. Note that the lack of emission in northwestern direction, seen near the spider, is an artifact. The image size is $12''$ squared. North is up and east is to the left.

5.1.5. HD 169142

HD 169142 (A5Ve: Dunkin et al. 1997a) is located at a distance of $d = 145$ pc (Sylvester et al. 1996). It has sometimes been recognized as a Vega-like star (e.g., Sylvester et al. 1996), like other old Herbig Ae stars, such as HD 150193, HD 144432, and HD 139614. However, its location on the H–R diagram, optical spectra, and the IR excess resemble those of Herbig Ae/Be stars with several million years of age (Dunkin et al. 1997a; Meeus et al. 2001), and hence it is considered to be in a PMS phase. H-band imaging polarimetry was initiated by Kuhn, Potter, and Parise (2001), and they detected the polarized intensity attributed to the circumstellar dust distribution. Significant polarization found out to a radius of $1\farcs5$ strongly encouraged us to observe HD 169142. The CO Keplerian disk was also reported, with an outer radius of $1\farcs6$ and an inclination of 13° (Raman et al. 2006; Panić et al. 2008). Grady et al. (2007) presented HST/NICMOS imagery at 1.1 μm, where the circular face-on disk was traced out to $1\farcs4$ in scattered light.

The circumstellar emission was revealed in $0\farcs8 \leq r \leq 1\farcs38$ (down to the $2\,\sigma$ level) after PSF-subtraction, as shown in figure 2. The observed outer radius of 200 AU, if adopting the distance $d = 145$ pc, is typical as a circumstellar disk around a PMS star. The more extended optical nebula does not exist around HD 169142, which also leads to an interpretation that the observed emission is scattered light originating from a circumstellar disk. The disk is almost circular, indicating a nearly face-on geometry, which is consistent with spatially resolved submillimeter observations ($i = 13° \pm 1°$: Raman et al. 2006) as well as with the low $v\sin i$ ($55\,\mathrm{km\,s^{-1}}$: Dunkin

Table 3. Non-detections.

Source	H (mag)	FWHM ($''$)	Exp. time (min)	Detection limit (2σ) (mag arcsec^{-2})	Flux ratio
HD 144432	6.5	0.″21	0.7	16.0 ($r \geq 2.''0$)	$< 4 \times 10^{-3}$
KK Oph	7.3	0.″10	10.3	16.7 ($r \geq 3.''5$)	$< 4 \times 10^{-3}$
HD 190073	6.6	—	2.3	16.5 ($r \geq 2.''5$)	$< 6 \times 10^{-3}$
HD 200775	5.5	0.″10	10.0	16.1 ($r \geq 2.''5$)	$< 2 \times 10^{-3}$
HD 218396	5.2	—	18.3	16.0 ($r \geq 2.''5$)	$< 8 \times 10^{-4}$
MWC 480	6.3	—	6.6	16.2 ($r \geq 2.''5$)	$< 2 \times 10^{-3}$
HD 34282	8.5	—	8.5	17.3 ($r \geq 2.''0$)	$< 1 \times 10^{-3}$
HD 131885	6.7	—	15.5	17.7 ($r \geq 2.''0$)	$< 3 \times 10^{-4}$
HD 139614	7.3	0.″11	8.8	17.9 ($r \geq 2.''5$)	$< 8 \times 10^{-4}$
HD 149914	5.8	—	5.6	17.1 ($r \geq 3.''5$)	$< 5 \times 10^{-4}$
VV Ser	7.5	0.″11	18.0	18.5 ($r \geq 3.''5$)	$< 6 \times 10^{-4}$
HD 176386	6.8	—	4.2	17.1 ($r \geq 5.''0$)	$< 2 \times 10^{-3}$
HD 179218	6.6	0.″11	15.5	18.2 ($r \geq 3.''5$)	$< 6 \times 10^{-4}$
HD 184761	6.1	0.″094	17.3	18.9 ($r \geq 5.''0$)	$< 1 \times 10^{-3}$
HD 191089	6.1	0.″11	12.2	18.0 ($r \geq 4.''5$)	$< 9 \times 10^{-4}$

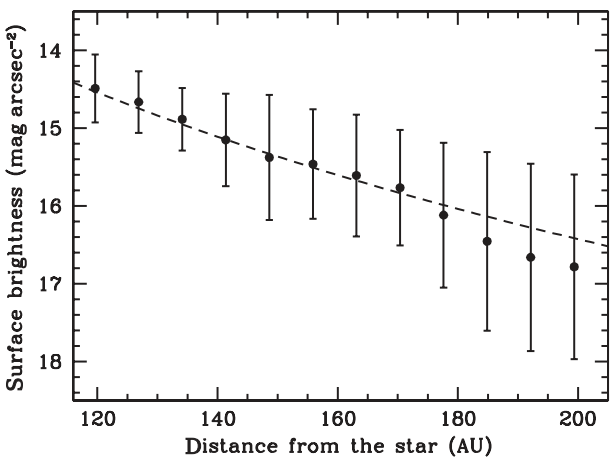

Fig. 3. H-band radial surface brightness distribution of the disk around HD 169142. The observed brightness was azimuthally averaged over 360°, except for the spider directions. A dashed line indicates the power-law index of −3.4. Error bars show the dispersion of brightness over the radial width of 0.″15.

et al. 1997b). The size and geometry of the disk are also in good agreement with a polarization map by Kuhn, Potter, and Parise (2001), and with a 1.1 μm image by Grady et al. (2007). Figure 2 suggests that the disk is brighter in the southwest than in the northeast. The brightness asymmetry is frequently ascribed to a scattering phase function when the contrast is seen along the minor-axis of the ellipse, since the forward scattering would be dominant. However, the brightness distribution of a face-on disk could be susceptible to the position match of the PSFs, and it was in fact varied even with a 0.2 pixel shift. Although Raman et al. (2006) derived the position angle of the inclined system to be $5° \pm 5°$, which is not inconsistent with our images, we hesitate to say that the western part is the near-side to us. The registration error does change the azimuthal brightness distribution, but it does not alter the disk size or its morphology.

Figure 3 shows the azimuthally averaged surface brightness profile. The fitting of a power-law function gave a slope of $r^{-3.4\pm0.4}$ with a large uncertainty, estimated by changing the radial range for the fitting and considered the PSF-subtraction using the reference star. Ignoring the steeper outskirts in $r \geq 1.''2$, we obtained $r^{-3.0\pm0.2}$, which is in good agreement with the slope measured in the optical region (Grady et al. 2007).

Adopting $H = 7.0$ mag for the brightness of HD 169142 (Malfait et al. 1998), the flux ratio of the scattered light and the total stellar light was calculated to be $F_{\rm disk}/F_{\rm total} = (1.5 \pm 0.2) \times 10^{-3}$. The scattered light was integrated in the radial range of $0.''85 \leq r \leq 1.''38$ ($= 123$ AU $\leq r \leq 200$ AU), with the pixel counts interpolated in the region where the spider pattern affected the image. The fractional luminosity of scattered light is much smaller than those obtained for AB Aur, HD 142527, and HD 150193, but larger than that for HD 163296.

5.2. *Non-Detections*

Out of 20 observed sources, disks around 15 stars were not spatially resolved. HD 149914, HD 184761, and HD 191089 show the shallower radial slopes of the residuals, but these are most likely due to the imperfection of the PSF subtraction. The circular residual around HD 149914 is likely to be caused by differences in the PSF shapes between HD 149914 and its reference star. For HD 191089, which was observed on June 4 and 6 in 2004, the observations on the first night suggested the circumstellar material distributed in the northern half direction, extended out to $r \sim 2.°5$. The second dataset, taken on June 6 also showed a similar feature, although the seeing condition was worse. However, a careful inspection of the data frames indicated that the spatial distribution slightly changed with time in the first dataset. Therefore, we concluded that the emission was likely to be an artifact, not the real one.

In the vicinity of the star, the halo suppression depends on the brightness of the central star and the PSF size (spatial

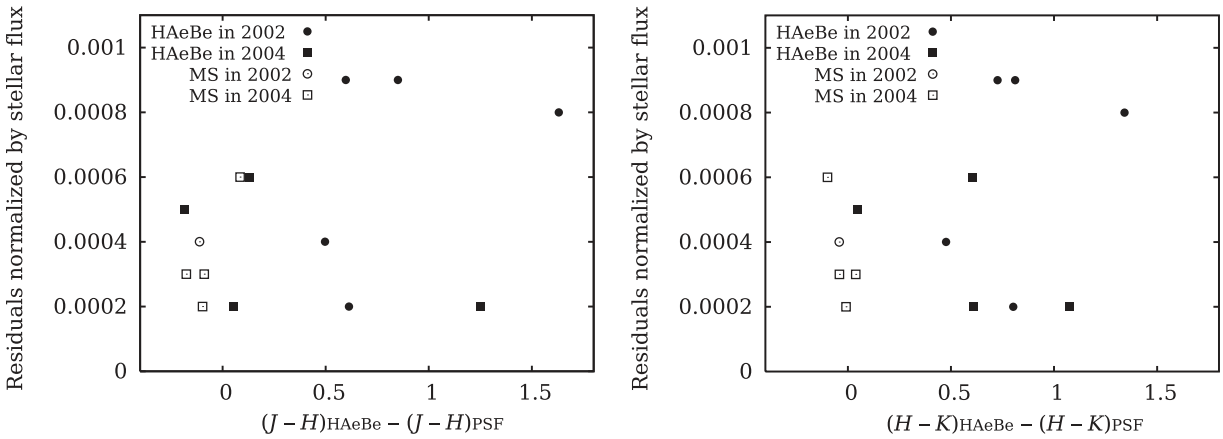

Fig. 4. Residual emission as a function of the difference of the NIR color between the science target and the PSF reference star.

resolution) as well as PSF matching, both of which are listed in table 3. The tabulated PSF sizes are the FWHMs of unocculted point sources in the FOV. There is no such point sources in some cases due to the small (22″) FOV of CIAO, but the intensity ratio of the peak and the halo suggested that the FWHMs were comparable to those with 0.″1 PSFs. Therefore, all sources have similar resolutions ($\sim 0.''1$), except for HD 144432 (0.″2). In the outer region where the residual emission reaches the noise level, the $2\,\sigma$ intensity is sufficient to distinguish the presence of a disk. We confirmed this by placing an artificial disk having a constant intensity of $2\,\sigma$ with $1\,\sigma$ noise in the PSF-subtracted image. The $2\,\sigma$ detection limit is shown on each object in table 3.

In the last column in table 3, the brightness ratio between the positive residual and the central star is shown. The residual emission was integrated over a whole azimuthal direction from the inner radius of 0.″5 or 1.″0 for targets observed before or after 2004, respectively, depending on the mask size. For HD 34282, the integration started from 0.″8. The residual flux should be increased when there was a mismatch of PSFs between the target and the reference star. Grady et al. (2009) demonstrated that a good color match between a science target and PSF stars is critically important based on the HST data. The ground-based observations suffered from a PSF variation due to a temporal change of seeing, which can be another cause of the PSF mismatch. Figure 4 compares the residual flux ratio integrated over $r = 1.''0$–$2.''0$ and the NIR color difference. A few young excess stars which are red in NIR have a larger color difference, and at the same time higher residuals. In addition, those were observed in 2002. The seeing size and its variation were worse in 2002 July than 2004 June on average, leading the poor quality of PSF-subtraction. HD 218396, however, was targeted when the seeing was much improved, and a better detection limit was achieved (see also table 3). HD 163296 has a relatively large color difference from the reference star [$\Delta(J-H) = 0.403$, $\Delta(H-K) = 0.657$], but it was imaged under decent seeing in 2004, resulting in the detection of a very faint disk. In addition, the *mismatch* frequently appeared as the difference in the elongation of the entire PSF shape or in the FWHM (peak to halo ratio). This is not expected from the color difference, which will result in diffraction spikes exhibiting banding in the subtracted image (C. Grady 2009, private communication). Therefore, we conclude that the seeing effect overcame the color difference in our observations. Imaging using higher-order AO will generate much better PSF, and the color difference could be an issue.

Columns 5 and 6 in table 3 also demonstrate that the detection limit is not uniform among sources at all. For the resolved disks, the typical ratio of the scattered to total flux is of on the order of 10^{-2}, if it is bright and optically thick (see subsection 5.1). On the other hand, optically thin disks have a ratio on the order of 10^{-3} or less (Weinberger et al. 1999; Schneider et al. 1999). Therefore, it was possible in 2004 to detect optically thin or fainter optically thick disks with a flux ratio of 10^{-3}, but no such disks were newly found in our limited sample, except for HD 163296, which has already been resolved in sensitive optical imaging (Grady et al. 2000).

The averaged radial profile normalized by the stellar fluxes is shown in figure 5 for each of the sources observed with a 0.″5 diameter mask, and those with a 1.″0 mask. The normalized brightness, corresponding to the contrast, differs between two datasets. Although the seeing was worse in 2002, HD 218396 was observed under better conditions, and hence it has a similar contrast with that observed in 2004 June. On the other hand, HD 190073 and KK Oph observed under bad seeing conditions have a smaller contrast, and they degrade the averaged contrast curve in figure 5. Therefore, the obtained contrast is little dependent on the mask size, at least between 0.″5 and 1.″0 masks, but strongly dependent on the quality of PSF-subtraction, determined by the temporal variation of the observed PSFs.

Non-detection means that the disk is faint or compact ($r \lesssim 1''$–$2''$). Dent, Greaves, and Coulson (2005) reported disk outer radii based on ^{12}CO (3–2) observations for some of our targets; in fact, the boundary of our detection/non-detection lies around a radius of 1″. We can, however, rule out a small disk for MWC 480, for which the extended disk has been resolved by millimeter observations (Mannings & Sargent 1997).

5.3. *Nearby Point Sources*

One of the useful by-products of high-resolution imaging is the detection of companion candidates in the vicinity of

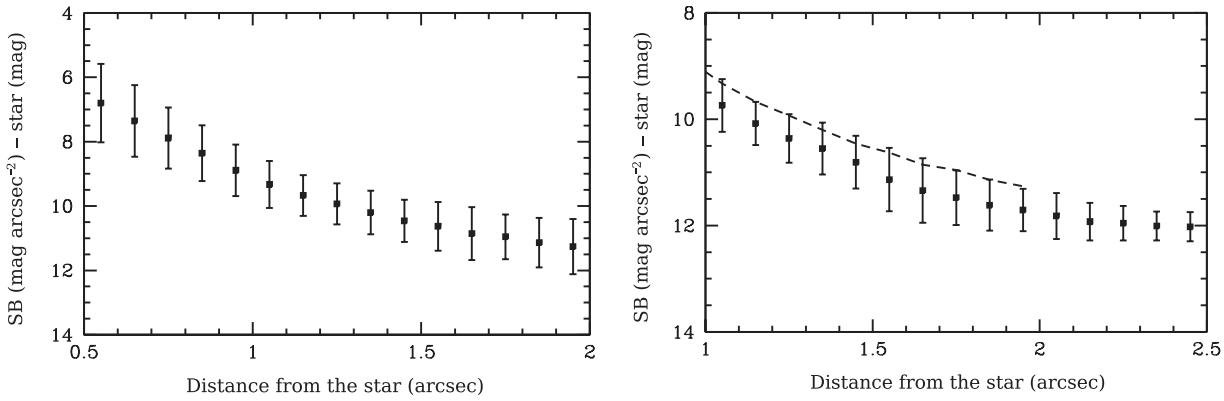

Fig. 5. Radial surface brightness averaged for six sources observed with a 0.″5 mask (left) and eight sources with a 1.″0 mask (right) in diameter. No circumstellar emission was found for these sources. The profile is normalized by the brightness of each central star. The error bars represent the dispersion among sources. Beyond $r = 2.''0$ (left) and $r = 2.''5$ (right), the brightness begins to reach the background level for several sources. The dashed line overplotted in the right image shows the profile in the left image. The difference is due to the quality of PSF-subtraction rather than the mask size (see, text).

Table 4. Nearby point sources.*

Source	Separation	P.A.	H (mag)	ΔH (mag)	Other reference†
HD 144432 B	$1.''49 \pm 0.''01$	$5.°7 \pm 0.°3$	9.48 ± 0.08	2.9	1
HD 150193 B	$1.''10 \pm 0.''03$	$225.°0 \pm 0.°8$	8.66 ± 0.05	2.3	1
KK Oph B	$1.''63 \pm 0.''01$	$245.°7 \pm 0.°3$	9.22 ± 0.02	1.6	1
KK Oph C	$5.''799 \pm 0.''005$	$270.°1 \pm 0.°2$	12.02 ± 0.04	4.6	
HD 200775 B	$2.''58 \pm 0.''01$	$168.°1 \pm 0.°2$	9.69 ± 0.06	4.2	2
HD 200775 C	$5.''91 \pm 0.''01$	$33.°6 \pm 0.°2$	12.14 ± 0.07	6.6	
HD 131885 B	$2.''19 \pm 0.''01$	$284.°0 \pm 0.°5$	saturated	—	
HD 139614 B	$4.''230 \pm 0.''008$	$302.°2 \pm 0.°5$	17.6 ± 0.1	10.3	3
HD 142527 B	$5.''56 \pm 0.''02$	$39.°7 \pm 0.°6$	14.47 ± 0.07	8.8	3
VV Ser B	$2.''541 \pm 0.''006$	$145.°8 \pm 0.°5$	16.8 ± 0.1	9.2	
HD 176386 B	$4.''09 \pm 0.''01$	$137.°6 \pm 0.°5$	saturated	—	4
HD 179218 B	$2.''539 \pm 0.''006$	$140.°6 \pm 0.°5$	13.20 ± 0.03	8.9	
HD 179218 C	$3.''600 \pm 0.''006$	$339.°6 \pm 0.°5$	15.48 ± 0.05	11.2	
HD 184761 B	$4.''390 \pm 0.''005$	$100.°5 \pm 0.°5$	13.47 ± 0.05	7.3	

* Relatively bright sources ($H < 18$ mag) within $6''$ are shown for the Herbig Aes located near the Galactic plane (KK Oph, HD 139614, VV Ser, HD 179218, and HD 184761). These nearby sources could be background objects, except for KK Oph B whose physical associations were confirmed (Pérez et al. 2004).

† 1. Carmona, van den Ancker, and Henning (2007), 2. Pirzkal, Spillar, and Dyck (1997), 3. our second epoch imaging confirmed that the candidate is a background object, 4. Stelzer et al. (2006).

a star. It is well known that most stars are born in binary or multiple systems. The multiplicity has an effect on the circumprimary disk if the separation is similar to the disk size predicted around a single star. In addition, the IR excess, which is an important indicator of circumstellar matter, may originate from photometrically unresolved companion stars. Therefore, knowledge of the multiplicity is important for studying the circumstellar dust distribution. Since Herbig Ae/Be stars are bright and distant, higher contrast is required to search for any less-massive companions near the star. Relatively deep imaging with AO has an advantage in finding fainter and closer companion stars.

The H-band magnitudes for nearby sources were measured via aperture photometry, in most cases using the APPHOT task in IRAF. For sources located where the PSF-subtraction residual was still dominant (VV Ser B), PSF-fitting photometry was performed using the DAOPHOT task. VV Ser was also observed in 2003 November, although not as deep as the observations in 2004, and two measurements were in agreement within an uncertainty of 0.1 mag.

Table 4 gives the sources detected in the same field of view of the targeted Herbig Ae/Be stars. The table includes companions known so far as well as new companion candidates. For Herbig Aes near the Galactic plane (VV Ser, KK Oph, HD 139614, HD 179218, HD 184761), only bright sources ($H < 18$ mag) within $6''$ are listed in the table. In the fifth column, the brightness ratio between the Herbig Ae/Be star and the nearby source is presented. The limitation of our observations is in obtaining images at one waveband at one epoch, providing only information concerning the existence

of nearby sources on the projected sky. Follow-up observations, such as multi-wavelength imaging, astrometry, or spectroscopy, are required to determine the physical connection to the Herbig Ae/Be stars (Carmona et al. 2007). X-ray observations with such as Chandra can reveal T Tauri companions, since they are often as bright as Herbig Ae stars, and tend to have harder X-ray spectra. T Tauri star companions were detected, evidently as X-ray emitters for HD 144432, HD 150193, and HD 176386 (Stelzer et al. 2006, 2009).

Second-epoch observations for HD 139614 and HD 142527 were carried out in 2008 May and July. For HD 142527 B, the relative position has changed since 2004 by $(\Delta\alpha, \Delta\delta) = (-0\farcs057 \pm 0\farcs017, \ -0\farcs095 \pm 0\farcs021)$; the amounts are consistent with the proper motion of HD 142527 ($\Delta\alpha_{\rm PM} = -11.20\,{\rm mas/yr}$, $\Delta\delta_{\rm PM} = -26.13\,{\rm mas/yr}$). HD 139614 B shows a red color ($J = 17.8 \pm 0.1$ and $K = 17.3 \pm 0.1$), but its relative position has also changed by $(\Delta\alpha, \Delta\delta) = (-0\farcs064 \pm 0\farcs010, -0\farcs103 \pm 0\farcs006)$, where this change is consistent with the proper motion for HD 139614 ($\Delta\alpha_{\rm PM} = -16.70\,{\rm mas/yr}$, $\Delta\delta_{\rm PM} = -26.80\,{\rm mas/yr}$). Therefore, HD 142527 B and HD 139614 B are likely to be background stars.

5.4. Color in Scattered Light

AB Aur and HD 142527 were observed not only in the H band, but also in J and/or K, which allows us to examine the disk colors in scattered light. The fractional disk fluxes in J and/or K are given in sub-subsection 5.1.1 for AB Aur and Fukagawa et al. (2006) for HD 142527. Given the small fraction of scattered light, we assume that the total flux represents the flux from the illuminating source including the thermal emission near the star as well as direct stellar light. For AB Aur and HD 142527, the integrated disk flux gave the same fractional luminosity in the H and K bands, suggesting that dust grains that reside where scattered light can be traced are typically larger than the interstellar grains. On the other hand, the color for AB Aur is marginally bluer in $J - H$, implying that wavelengths shorter than $1.6\,\mu$m could probe the upper layer, where the small grains in the surrounding envelope may contribute to the scattering. Note that HD 100546, the Herbig Ae/Be star also with the large-scale nebulosity, shows the quite red color in optical like observed for Kuiper Belt objects, unlike for ISM (Ardila et al. 2007). The optically thick disks for Herbig Aes and T Tauri stars that have been resolved thus far generally appear to be gray in scattered light at NIR wavelengths (figure 6; Schneider et al. 2003; Weinberger et al. 2002; McCabe et al. 2002; Weinberger et al. 1999; Debes et al. 2008). A similar trend is seen for optically thin disks, HD 141569 A and HR 4796 A, but they are interestingly red in the optical region (Weinberger et al. 1999; Clampin et al. 2003; Debes et al. 2008). It has been suggested for HR 4796 A that the resemblance to outer solar-system objects may imply the presence of organic material around the star, although that is not a unique possibility to explain the observed color (Debes et al. 2008; Köhler et al. 2008). As can be seen in figure 6, however, the color remains nearly gray in the small wavelengths coverage in NIR for various kind of disks. Multi-waveband data from optical through NIR will be very useful to explore the property of scatterers. The source revealing the slightly red color, like HR 4796 A, is only GG Tau with the

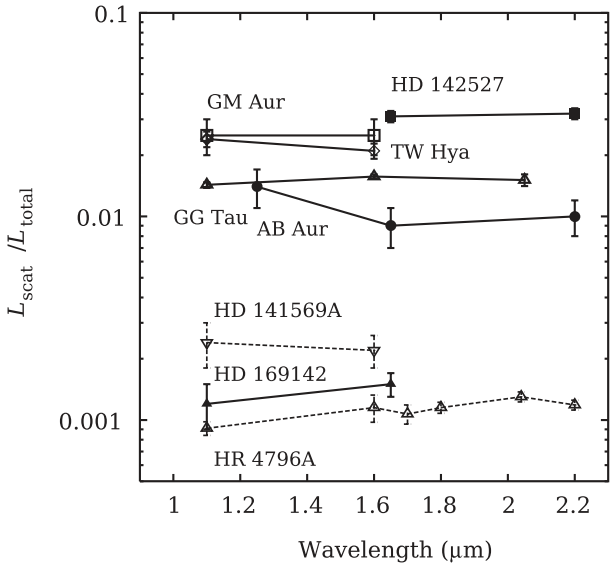

Fig. 6. Near-infrared color in scattered light (GM Aur, Schneider et al. 2003; TW Hya, Weinberger et al. 2002; GG Tau, McCabe et al. 2002; HD 141569A, Weinberger et al. 1999, Augereau et al. 2001; HR 4796A, Debes et al. 2008). The $1.1\,\mu$m brightness for HD 169142 is taken from Grady et al. (2007), and the stellar flux was estimated using CALCPHOT task in SYNPHOT package with the Kurucz model assuming $T_{\rm eff} = 7800\,{\rm K}$ and $g = 4.5$. The mutli-wavelength data were taken with the same instrument except for HD 169142. The disk-scattered light was integrated outside of the occulting mask for coronagraphy, meaning that the fractional luminosity is considered to be a lower limit.

$J - H$ significantly (3.5σ) larger relative to the star. Basically, without introducing organic compounds or the right porosity to reproduce the red scattering, the scattered light should be blue or neutral, depending on the grain size if the scattering is dominated solely by albedo. McCabe, Duchêne, and Ghez (2002), however, showed that considering the disk inclination and the scattering asymmetry, which is dependent on the wavelength, the red color can be produced in the optically thick disk. We also note that the color in figure 6 is derived from the integrated flux, but the spatial variation in the color has been found for some disks (e.g., Ardila et al. 2007).

5.5. Disk Luminosity in Scattered Light

In table 5, we summarize the observed properties of the resolved disks: the normalized disk luminosity at $1.6\,\mu$m, the disk radii where the scattered light was detected, the radial dependence of the surface brightness, and the derived inclination assuming a circular disk. The disk around HD 100546 is included in the table, since it has been resolved at $1.6\,\mu$m (Augereau et al. 2001). We also added three optically thin disks and another 3 disks associated with classical T Tauri stars for a comparison.

In order to compare the disk luminosities for sources with various distances and mask sizes, we recalculated the fractional disk luminosity, adopting 50 AU as an inner radius. The measured radial slope was extrapolated to the inner region for HD 150193, HD 169142, and AB Aur, assuming that there is no gap or inner hole. The observed outer radius could be controled by the sensitivity, particularly for our imaging; thus,

Table 5. Resolved disks in scattered light at 1.6 μm.

Source	$L_{\rm scat}/L_{\rm total}$ (1.6 μm)	Radial range (AU)	Radial slope*	i (°)	Reference†
HD 150193	$(1.3\pm0.3)\times10^{-2}$	59–225	$-4.6\ \pm0.1$	$38\ \pm9$	1
HD 169142	$(1.5\pm0.2)\times10^{-3}$	123–200	$-3.4\ \pm0.4$	nearly face-on	1
AB Aur	$(1.2\pm0.2)\times10^{-2}$	120–580	$-3.0\ \pm0.1$	$30\ \pm5$	1
HD 142527	$(3.1\pm0.2)\times10^{-2}$	105–420	$-6.6,\ -8.9$	—	1
HD 100546	$(1.6\pm0.2)\times10^{-2}$	46–380	-2.92 ± 0.04	$51\ \pm3$	2
HD 163296	$\sim2\times10^{-4}$	232–430	—‡	~45	1
HD 141569 A	$(2.2\pm0.2)\times10^{-3}$	190–891	—‡	$51\ \pm3$	3
HR 4796 A	$(2.4\pm0.5)\times10^{-3}$	≥44	—‡	73.1 ± 1.2	4
β Pic	$(1.8\pm0.4)\times10^{-3}$	≥50	—	edge-on	1
GM Aur	$(2.5\pm0.5)\times10^{-2}$	49–700	-3.5	50	5
TW Hya	$(2.1\pm0.2)\times10^{-2}$	22–228	$-2.6\ \pm0.1$	4	6
GG Tau	$\sim1.5\times10^{-2}$	140–308	—§	$40\ \pm2$	7

* Radial dependence of surface brightness ($r^{\alpha_{\rm s}}$). The index $\alpha_{\rm s}$ is measured in the radial range in column 3 or in a part of the region.
† 1. This work, 2. Augereau et al. (2001), 3. Augereau et al. (1999), 4. Schneider et al. (1999), 5. Schneider et al. (2003), 6. Weinberger et al. (2002), 7. McCabe, Duchêne, and Ghez (2002).
‡ Circumstellar disk but with a ring morphology.
§ Circumbinary disk.

$r = 400$ AU was tentatively assumed, although the outer disk contributes little to the total disk luminosity. HD 150193 and HD 169142 have smaller outer radii, but the contributions from the assumed outer parts were negligible. We therefore did not truncate the disk at a certain radius for larger disks. For instance, the outer disk of GM Aur (400 AU $\leq r \leq$ 700 AU) and AB Aur (400 AU $\leq r \leq$ 580 AU) contribute below 1% and about 3% of the total luminosity, respectively.

For HD 150193, there exists a flat distribution near the coronagraphic mask in its radial profile (Fukagawa et al. 2003). If it is real, the extrapolation of the brightness distribution follows $I(r) \propto r^{-2.1}$, derived from a power-law fitting in $r < 0\farcs55$ ($= 83$ AU). The difference is large, by over 2 times, between the disk luminosity using this shallower slope and that with steeper one for the outer part ($\alpha_{\rm s} = -4.6$). The value with the flatter inner distribution was assumed in the later discussion. The circumstellar disk for TW Hya was observed with 22 AU as the inner radius. Since the inner disk can strongly alter the disk luminosity, we subtracted the scattered light arising from inside 50 AU. According to figure 3 in Weinberger et al. (2002), the brightness distribution is deviated from the power-law, and is almost flat at $r \lesssim 0\farcs7$ ($= 40$ AU). Therefore, the disk luminosity at $r \leq 40$ AU was estimated assuming an annulus with a constant intensity, 5 mJy arcsec^{-2}. The luminosity of this annulus and the subsequent distribution with the slope of $\alpha_{\rm s} = 2.6$ in $r =$ 40–50 AU were added together, resulting in 41% of the total observed luminosity. The fractional luminosity outside of 50 AU was estimated to be $(1.4\pm0.3)\times10^{-2}$, and we used this value for a later comparison of the scattered light luminosity with various stellar parameters. For HD 163296, we adopt here the upper limit of 2×10^{-4} as the fractional luminosity (see sub-subsection 5.1.4). Since the central star is much brighter than the disk, the fractional luminosity is less susceptible to the assumed brightness in the disk annulus. However, note that the variability of the surface brightness (Wisniewski et al. 2008) turns into the variability of the fractional luminosity. Under a crude assumption that the disk could be brighter by 1 mag arcsec^{-2}, as seen in the optical images (Wisniewski et al. 2008), the noticeable faintness still remains for HD 163296. The variable shadowing hypothesis suggests that the brighter the outer disk is in scattered light, the fainter is the inner disk in thermal emission. However, Sitko et al. (2008) did not detect a significant ($> 10\%$) change in the NIR excess from 1998 to 2006, except for 2002, which also makes the disk to be the faintest. For the other ring-like disks (HD 141569 A, HR 4796 A, HD 142527, GG Tau), we took the observed values (table 5).

5.5.1. Stellar age

Figure 7 shows the fractional luminosity of scattered light relative to the stellar age. The PMS age was estimated using the theoretical evolutionary track by Palla and Stahler (1999). $T_{\rm eff}$ and L_* were derived from the spectral type and by integrating the Kurucz model. The uncertainty of the derived age arises from the uncertainties of $T_{\rm eff}$, L_*, and isochrones. In our derivation, there is a typical error of a few million years. Other factors affecting L_* are the distance, extinction, and variability. The uncertainties of ages are thought to be larger for sources with uncertain distances (VV Ser, HD 190073), larger extinctions (VV Ser, KK Oph), and lager variations (VV Ser, KK Oph). Moreover, note that the potential multiplicity may affect the estimation of the luminosity. HD 200775 is an earlier type star (B3), for which we did not attempt to derive the age using the evolutionary track as the massive star evolves rapidly and the inferred age is considered to be more ambiguous (cf. 0.1 ± 0.05 Myr, $10.7\pm2.5\,M_\odot$: Alecian et al. 2008). It is noted that we assumed the solar metallicity for simplicity, since metallicity measurements for early-type young stars are very difficult. However, note that it might give an inappropriate age if the true metallicity is different, as demonstrated for HD 34282 (Merín et al. 2004).

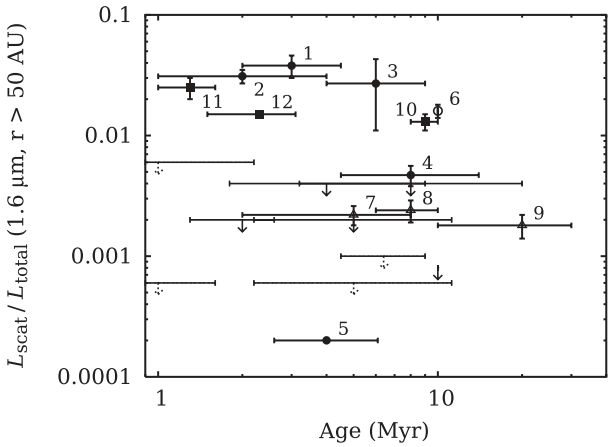

Fig. 7. Fractional luminosity of disk scattered light versus stellar age. Filled circles (observed sources) and an open circle (HD 100546: Augereau et al. 2001) indicate the optically thick disks around Herbig Ae/Be stars. Other optically thin disks resolved around intermediate-mass stars are collected from literature and shown with triangles (see table 5 for references). Sources without circumstellar emission in our observations are also presented (solid arrows for $d < 200$ pc, dashed arrows for $d > 200$ pc). Filled squares indicate the optically thick resolve disks around T Tauri stars (table 5). 1. AB Aur, 2. HD 142527, 3. HD 150193, 4. HD 169142, 5. HD 163296, 6. HD 100546, 7. HD 141569 A, 8. HR 4796 A, 9. β Pic, 10. TW Hya, 11. GM Aur, 12. GG Tau.

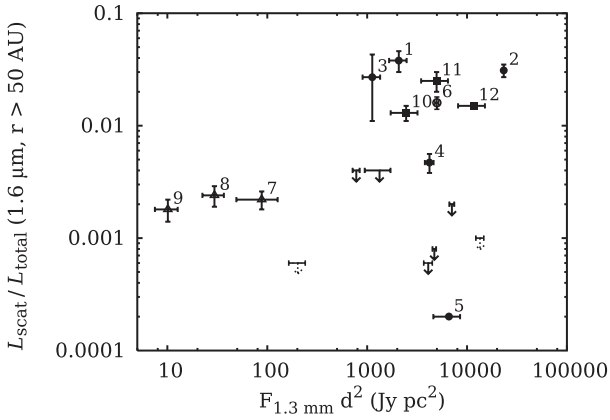

Fig. 8. Fractional luminosity of disk scattered light relative to the 1.3 mm continuum flux. The 1.3 mm fluxes are taken from the literature (Alonso-Albi et al. 2009; Acke & van den Ancker 2004 and references therein). For HR 4796 A, the flux at 1.3 mm is estimated using the observed 850 μm flux (Greaves et al. 2000) and $\alpha = 2.5$ as the wavelength dependence of the flux, with the uncertainty of the measured flux and $\Delta\alpha = 0.5$. The unresolved sources at 1.6 μm are also plotted with the upper limits. The symbols are the same as used in figure 7.

Dunkin, Barlow, and Ryan (1997a) found underabundances of the relatively later-type stars HD 169142 (A5) and HD 139614 (A7) but within 0.2 dex. Therefore, we use the ages listed in table 1 for the comparison with the disk luminosity in scattered light, except for HD 34282. The age determination for main-sequence stars is more problematic. Different ages for the same star are inferred sometimes by over an order of magnitude, depending on the derivation method, such as the location in the H–R diagram for early-type stars, the rotational velocity, X-ray emission, the strength of chromospheric calcium emission lines for late-type stars (Lachaume et al. 1999). It would thus be safe to adopt the value only when consistency is obtained among several methods. For our targets, Zuckerman and Song (2004) tabulated the ages for HD 191089 and HD 218396, derived from multiple ways. Miroshnichenko et al. (1999) suggested the zero-age main-sequence (ZAMS) location for HD 184761.

In spite of these caveats for the ages and the limited number of samples, it would be worth attempting to find the age dependence of the detection rate in scattered light and the disk brightness. In figure 7, older sources near ZAMS (~ 10 Myr) have fainter disks compared with younger sources ($\lesssim 5$ Myr), except for HD 163296. In addition, there can be seen a larger variation in the scattered light for older sources ($\gtrsim 5$ Myr). The three fainter disks HD 141569 A, HR 4796 A, and β Pic possess optically thin (multiple-) ring-like disks. The formation of a ring structure is often related to an evolutionary effect. The grain growth is enhanced in the inner denser disk and large bodies (protoplanets, large planetesimals) effectively perturb small planetesimals, which enhances the collisional reproduction of grains and forms the bright ring (e.g., Kenyon & Bromley 2004). For optically thick disks, there is no clear trend in the disk brightness with the stellar age. This is not unusual, since the absence of a correlation between stellar age and many of disk parameters has been frequently found (e.g., Kitamura et al. 2002). Figure 7 also suggests that the the scattered light luminosity is at a similar level for T Tauri stars ($M_* \sim 0.7\,M_\odot$, White et al. 1999; Webb et al. 1999) and intermediate-mass stars.

5.5.2. Millimeter emission

The luminosity in scattered light is shown as a function of the 1.3 mm flux in figure 8. The 1.3 mm dust continuum is translated to the disk mass, assuming the dust opacity, temperature, and gas-to-dust mass ratio. The lack of sources at the top-left is considered to be real, but that seen at the bottom-left (the smaller fluxes and disk luminosities) could be due to the small number of observed stars, since the detection rate itself is low for Vega-like stars. Since we tend to pick up the brightest disks, these disks are considered to give an upper limit of the disk brightness in scattered light.

Among Herbig Ae stars with optically thick disks, figure 8 implies that the circumstellar dust mass is not correlated with the detection rate of extended disks in scattered light. This characteristic has been well known for such as MWC 480, which is very bright and extended in millimeter, but hard to detect in scattered light. This has been interpreted as being related to the degree of disk flaring. In scattered light, we can probe the surface layer but not the disk midplane if the disk is optically thick. When the disk is highly flared, the bright disk is detected since the flared surface efficiently receives the radiation from the central star. On the other hand, the flat disk cannot be seen in scattered light, but can be detected in thermal emission since the dust grains do exist around the equatorial plane. In addition, no tendency is found in the scattered light luminosity with 1.3 mm flux among the resolved sources, suggesting that the surface density of small grains in the upper layer and/or the surface structure to be illuminated cannot be determined simply by the total mass of the disk.

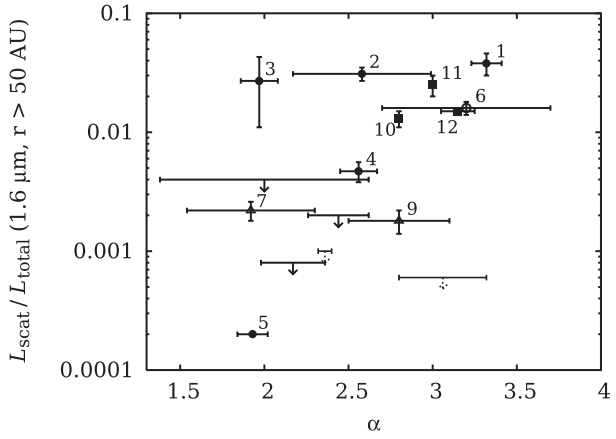

Fig. 9. Scattered light luminosity and spectral index α. The meanings of symbols are the same as in figure 7.

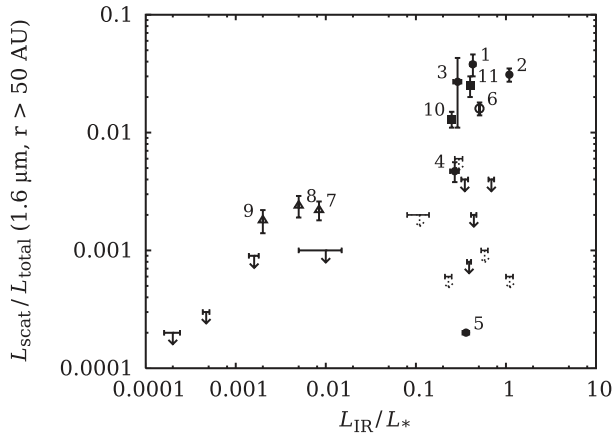

Fig. 10. Fractional luminosity of disk scattered light as a function of IR excess. The meanings of the symbols are the same as in figure 7.

5.5.3. *Millimeter spectral index*

The spectral index in the millimeter SED (α, where $F_\nu \propto \nu^\alpha$) represents the size of dust grains, and hence may be related to the disk brightness in scattered light. The radiation becomes optically thick if the grains are larger than the observing wavelengths. Consequently, the slope becomes closer to the Rayleigh–Jean tail of the black body, $\alpha \sim 2$, while for the ISM grains, $\alpha \sim 4$ is expected (Miyake & Nakagawa 1993). In figure 9, the disk luminosity in scattered light is shown against α collected from the literature (Acke et al. 2004; Schneider et al. 2003; Guilloteau et al. 1999; Calvet et al. 2002). There can be seen a rough trend that the larger is α, the brighter is the disk in scattered light. HD 179218 is an exception, which has a steeper slope in the millimeter SED, but has not been resolved in our observations. The non-detection might be due to its larger distance ($d = 240$ pc) and its disk size which has been predicted to be about 0.″5–0.″8 (Dent et al. 2005; Panić & Hogerheijde 2009). HD 163296 shows small α, and has the faintest disk in scattered light. Two sources, AB Aur and HD 100546, have large α, and their outer disks are bright. The IR spectra also suggest the difference of dust sizes for these sources. The presence of large cold dust grains is inferred by the color temperature in the spectra of HD 163296, whereas it is absent in AB Aur and HD 100546 (van den Ancker et al. 2000). The dusty material around AB Aur and HD 100546 show the spiral structures and they are surrounded by large-scale (> 1000 AU) nebulosities. The flesh dust grains from the envelope could contribute to the large α, or the measurements at (sub)millimeter wavelengths could be contaminated from the envelope with single-dish telescopes. It is important to keep in mind that the presence of the outer nebulosity does not necessarily mean that the system is young, as discussed in sub-subsection 5.5.7.

5.5.4. *IR excess*

The fractional luminosity of the IR excess ($\tau = L_{\rm IR}/L_*$) is derived from the SED by integrating the excess flux after subtracting the fitted Kurucz model (table 1). We integrated the excess flux from the onset wavelength 1 μm to 2.7 mm. The Herbig Ae/Be stars have NIR excesses as well as far-infrared (FIR) excesses, except for HD 149914 and HD 176386. Most Herbig Ae stars have both NIR and FIR excesses on the order of 10^{-1}, which is attributable to the presence of an optically thick disk. Note that a few sources have $\tau > 1$ (VV Ser, HD 142527), which may not be reconciled with the purely reprocessing disk. There seems to be another heating source in these systems, such as the active accretion or unseen red companions. HD 176386 has little NIR emission and sometimes shows the Hα absorption, suggesting that the star is more evolved, as well as HD 149914. The well-known Herbig Ae/Be star with only FIR excess component is HD 141569 ($\tau = 8.4 \times 10^{-3}$), which is considered to be a transitional object to the Vega-like phase. Three Vega-like stars, HD 131885, HD 191089, and HD 218396, have no NIR excesses. For these stars, the excess was calculated based on the black body fit ($T_{\rm BB} = 110$, 100, 50 K for HD 131885, HD 191089, and HD 218396, respectively). HD 184761 has a considerable excess at 12 μm, and the excess declines steeply toward FIR. We estimated the excess flux using the hotter dust ($T_{\rm BB} = 370$ K), which is quite warmer than typical Kuiper-belt type disks.

In figure 10, the scattered luminosity is shown with the IR excess. A similar trend is found as that in the previous comparison with 1.3 mm flux (figure 8). The absence of sources in the top-left, where sources have both a small IR excess and a bright disk, is reasonable and considered to be real. The bright disks with $L_{\rm scat}/L_{\rm total} \sim 10^{-2}$ are not found around the stars with $L_{\rm IR}/L* < 10^{-2}$. As is obvious in figure 10, the disk luminosity, as well as the detection rate, is independent of the IR excess for Herbig Ae stars. This could be plausible, since the luminosity of IR excess cannot be an ideal indicator of the radial and vertical extent of the disk structure. If the detection rate is determined by disk flaring, we might see the correlation between the disk luminosity and parameters related to the flaring. Meeus et al. (2001) proposed the SED classification on the disk geometry: flared (group I) and flat (group II) disks. Sources in group I and II show a similarity in NIR ($\lesssim 2\,\mu$m) but a difference in FIR. A group I SED can be fitted by a power-law continuum plus an additional black body for a strong excess in FIR, which could be caused by an outer flared surface of the disk. Meanwhile, the IR part of the

group II SED is roughly represented only by a power law. The classification was attempted using the ratio of the NIR to FIR flux and the IRAS color [12] − [60] (van Boekel et al. 2003) (figure 11). The flat outer disk shadowed by the inner rim cannot be detected in scattered light, and the scale height of the inner disk controls the degree of shadowing. Indeed, the group I disks show higher detection rates in scattered light than the group II (table 6). In addition, the group I disks with large flux ratios of between 30 and 13.5 μm (Acke et al. 2009) may tend to be detected in scattered light, except for a distant one, HD 34282. However, $L_{\rm scat}/L_{\rm total}$ is not correlated to the IRAS color or FIR excess, nor to the flux ratio of 30 and 13.5 μm.

5.5.5. PAH emission

The emission features of PAH (Polycyclic Aromatic Hydrocarbons) molecules have been observed for many of circumstellar disks around Herbig Ae/Be stars. The PAH emission requires the molecules to be present where they are exposed to UV photons from the central star. Therefore, if the dust grains are well coupled with the gaseous disk, PAH emission could be better linked with the disk visibility in scattered light, rather than the silicate emission which originates from the inner part ($r \lesssim 10$ AU) (Habart et al. 2004). The correlation between the PAH emission and the group I/II classification, and at the same time, the absence of correlation between the stellar UV luminosity has been reported (Acke & van den Ancker 2004). We compiled scattered light imaging observations of Herbig Ae stars in table 6, and confirmed that the strong PAH sources belong to group I, and they tend to be resolved in scattered light. Figure 12 shows the scattered light luminosity as a function of the PAH line strength at 6.2 μm (considered to be least affected by the silicate emission) or 8.6 μm. To compare with Grady et al. (2005b), the PAH strengths were scaled to be at 100 pc. Given the large distances for non-detections in scattered light but with strong PAH features, there seems to be a correlation between the disk detection in scattered light and the PAH strength, consistent with Grady et al. (2005b). However, it should be noted that there are exceptions, and especially the relatively weak PAH for HD 142527 which has a remarkably bright and extended disk in scattered light is puzzling. One possible reason would be the weaker UV luminosity, since the spectral type of this star is F6. Alternatively, if the PAH strength is related to the area where molecules can be UV-excited, the wide gap and the steep outer profile seen in scattered light for HD 142527 may imply that the disk has a direct line of sight to the star only at the inner wall of the outer disk if the small inner disk is shadowed. The decoupling of gas and dust disks might have another effect, as Ohashi et al. (2010) detected significant gas depletion. The correlation between the scattered light and PAH emission is still seen with the 8.6 μm feature, but less conspicuous for 11.3 μm.

5.5.6. Binarity

The binarity has a significant effect on the disk structure in some cases. In particular, a companion star separated by 10–100 AU may alter the size of the circumstellar disks by tidal

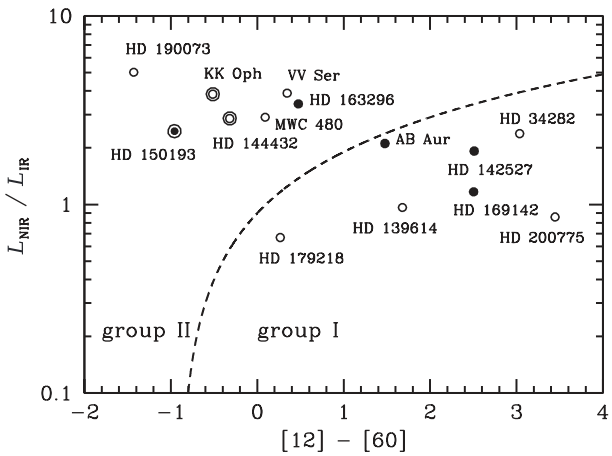

Fig. 11. NIR excess and FIR color for observed Herbig Ae/Be sources. Filled circles indicate the sources with resolved disks in scattered light, and open circles denote the non-detection. The dashed line presents $L_{\rm NIR}/L_{\rm IR} = ([12] - [60]) + 0.9$, which is the boundary between two groups, empirically found by Dullemond et al. (2003); van Boekel et al. (2003). Double circles show binaries with companions at ∼160–260 AU.

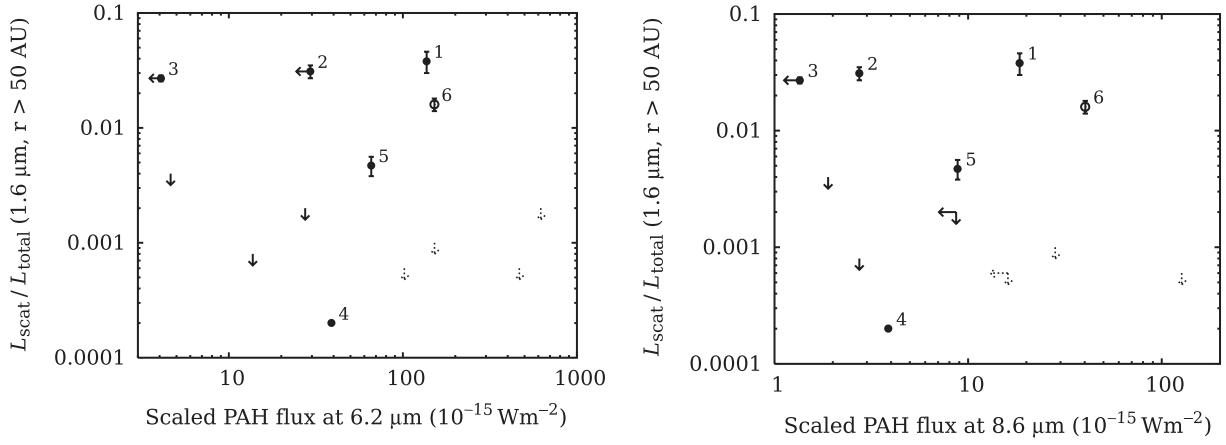

Fig. 12. Scattered light luminosity versus PAH strength at 6.2 μm (left panel) or 8.6 μm (right panel). The PAH measurements are from Verhoeff (2009), Keller et al. (2008) with Spitzer/IRS, and Acke and van den Ancker (2004) with ISO. The symbols are the same as in figure 7. Objects in these panels: 1. AB Aur, 2. HD 142527, 3. HD 150193, 4. HD 169142, 5. HD 163296, 6. HD 100546.

Table 6. Herbig Ae Stars in scattered light.*

Source	d (pc)	Scattered light	Reference†	PAH	Large-scale nebulosity	Companion
group I						
AB Aur	144	y	1	Y	y	—
HD 34282	350	n	1	y	n	—
HD 36112	200	n	2	—	n	—
CQ Tau	99	n	2	y	y‡	—§
HD 97048	180	y	9	Y	y	—
HD 100453	111	n	3	y	n	$\rho = 116$ AU
HD 100546	103	y	4, 5	Y	y	—
HD 135344	84	y	6	y	n	—
HD 139614	140	n	1	y	n	—
HD 142527	140	y	1	y	y	—
HD 169142	145	y	1, 7	Y	n	—‖
HD 179218	240	n	1	Y	n	—
group II						
MWC 480	170	n	1, 6	y	n	—
HD 95881	118	n	2	y	n	—
HD 104237	115	n	8	y	n	$\rho = 156$ AU
HD 142666	145	n	2	y	n	—
HD 144432	145	n	1	y	n	$\rho = 216$ AU
HR 5999	200	n	2	u	n	$\rho = 334$ AU
HD 150193	150	y	1	u	n	$\rho = 165$ AU
KK Oph	160	n	1	—	n	$\rho = 261$ AU
HD 163296	122	y	1	y	n	—
VV Ser	310	n	1	y	n	—
HD 190073	> 290	n	1	—	n	—

* Column 5 (PAH): "Y" means that the PAH feature was detected with the line flux larger than 5×10^{-14} W m^{-2} at least at one of the wavelengths 3.3, 6.2, 7.7, 8.6 and 11.3 μm, while "y" indicates the weaker line (Verhoeff 2009; Keller et al. 2008; Acke & van den Ancker 2004). As for "u", an upper limit was obtained by ISO (HR 5999: Acke & van den Ancker 2004) or Spitzer (HD 150193: Verhoeff 2009). Column 6 (large-scale nebulosity): optical nebulae found in the Digitized Sky Survey (DSS) archival images. The tenuous nebula is detected with HST/STIS for HD 100546. Column 7 (companion): the *projected* separation is given in AU.

† 1. This work, 2. Grady et al. (2005b), 3. Collins et al. (2009), 4. Augereau et al. (2001), 5. Grady et al. (2001), 6. Grady et al. (2009), 7. Kuhn, Potter, and Parise (2001), 8. Grady et al. (2004), 9. Doering et al. (2007).

‡ The arc-like nebulosity was detected with HST/STIS, but it is smaller and much fainter than the nebula around HD 100546 (Grady et al. 2005a).

§ There is a companion candidate at $\rho = 188$ AU (Grady et al. 2005b).

‖ There is a T Tauri binary system at around 1350 AU which is comoving with HD 169142 at the 4σ confidence level (Grady et al. 2007).

truncation, and consequently the evolutionary timescale of the disks. A similar discussion is found in Grady et al. (2005b), but it would be worth pointing out that binaries with critical separations constitute a large portion of group II sources, while no such binary is found in group I (table 6). A truncation of an outer disk naturally produces the less FIR excess. Therefore a care must be taken in the discussion of the possible evolutionary trend deduced from the SED modeling for multiple sources. We have to await more statistical samples consisting of single stars, in order to observationally study the evolutionary sequence of the disk structure.

5.5.7. Inner disk property

The inner disk property can be a useful evolutionary clock, since the evolution likely proceeds inside-out. One of the indicators of youth is the mass accretion activity, which can be characterized with an equivalent width of the Hα emission line, EW(Hα). Although Hα usually shows strong variability, Manoj et al. (2006) demonstrated the overall decay of EW(Hα) with stellar age. In figure 13, however, there is no trend between the EW(Hα) and the disk luminosity in scattered light. HD 163296 is still actively accreting, but the disk is the faintest, while HD 142527 is brighter in scattered light, but fainter in Hα. On the other hand, AB Aur is bright both in scattered light and Hα. Ignoring binaries (HD 144432, HD 150193, KK Oph), no clear correlation is still found. Excluding relatively far sources (HD 34282, HD 179218, VV Ser) prevents us to discuss any trend, since the remaining sample size is too small, but even in that case the non-detection of the disk for MWC 480 which has the similar EW(Hα) to HD 163296 is remarkable. Our detection limit for MWC 480, although it is much higher than the brightness of the resolved disk around HD 163296, suggests that the disk should be very faint.

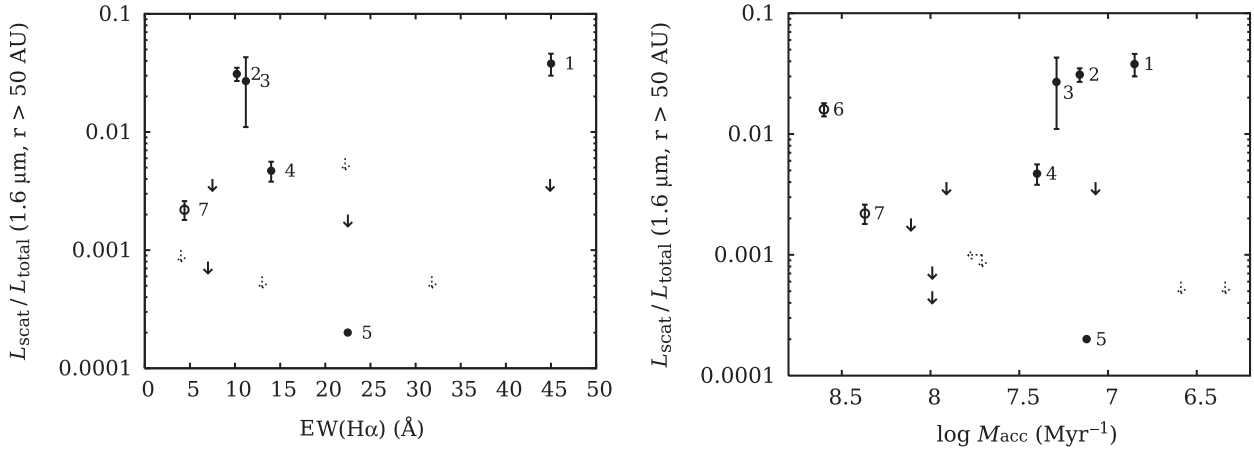

Fig. 13. Disk luminosity in scattered light versus Hα equivalent width (left panel) and mass accretion rate (right panel). The equivalent widths were taken from Manoj et al. (2006), and the estimates of accretion rates from Vieira, Pogodin, and Franco (1999) for HD 100546 and Garcia Lopez et al. (2006) for others. The symbols are the same as in figure 7. Objects in these panels: 1. AB Aur, 2. HD 142527, 3. HD 150193, 4. HD 169142, 5. HD 163296, 6. HD 100546, 7. HD 141569.

Therefore, it may be implied that both strongly or weakly accreting sources have flared outer disks, but stars in the intermediate stage are surrounded by flatter disks. A similar plot is shown in the right panel of figure 13 using the accretion rate estimated from the luminosity of the Brγ emission line (Garcia Lopez et al. 2006).

The inner disk can be characterized in a more comprehensive way by considering not only Hα, but also various signatures, such as presence of jets, inner cavities, or spectroscopic features. One common property for the resolved disks in scattered light is that they have the (signs of) inner holes/gaps (e.g., Grady et al. 2005b). Those are sometimes circumbinary disks with gaps opened by companions (GG Tau, UY Aur). As for stars that are believed to be single, the inner depletion has been suggested even with the high accretion rate for AB Aur (Piétu et al. 2005), the inner wide gap was observed for HD 142527, and an inner hole (0.″2–0.″3) has been suggested for HD 169142 (Grady et al. 2007). A tiny cavity ($r = 13$ AU) was also detected for HD 100546 (Grady et al. 2005a), which is a star close to ZAMS with a small accretion rate (Vieira et al. 1999) and showing significant crystallinity (Malfait et al. 1998). TW Hya also has an inner hole (e.g., Calvet et al. 2002). On the other hand, we do not see bright disks in scattered light for actively accreting stars, like HD 163296 and MWC 480. Therefore, those disks resolved in scattered light so far have a dust-depleted zone in the inner region, which might allow the outer disk to be illuminated.

5.5.8. Outer envelope

The large-scale nebulosity (envelope) is sometimes associated with stars in their ages of 10^6–10^7 yr. The Digitized Sky Survey (DSS) archival images show such nebulosity for AB Aur and HD 142527 in our sample. In addition, sensitive optical imaging by the HST/STIS has detected an envelope around HD 100546 (Grady et al. 2001), although the DSS image does not show it possibly due to its faintness. With high-resolution imaging, these three sources are surrounded by bright, structured outer disks in scattered light. The group I source HD 97048 is also surrounded by an optical nebula in DSS, and a spiral-like feature was found in an optical image obtained with HST (Doering et al. 2007). This makes the fraction of nearby Herbig Ae stars that have a large scale nebulosity to be ∼20% among 25 stars in Acke et al. (2004). Since they are not always young in terms of circumstellar structure (AB Aur, HD 100546, HD 142527), the difference in the lifetime of envelopes could depend on stellar isolation. The sources that had obtained substantial circumstellar material without close stellar passages might result in brighter and/or long-lived envelopes, thus disks.

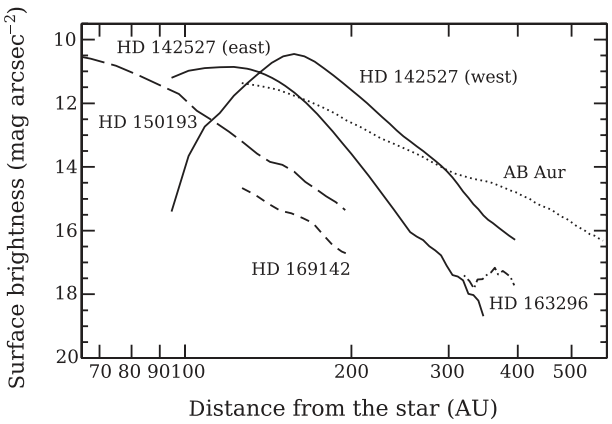

Fig. 14. Surface brightness profile for resolved disks.

5.6. Surface Brightness Distribution

The surface brightness distributions of scattered light in the five disks are shown in figure 14. In this plot, the brightness for HD 163296 was derived from the detected ansae, and it is to be taken as an upper limit. Also note that the temporal variation of the disk brightness has been known for HD 163296. For

HD 142527, the radial profile was measured along P.A. = 60° and shown for eastern and western disks separately in the figure (Fukagawa et al. 2006). For others, the profile was azimuthally averaged (Fukagawa et al. 2003, 2004).

The radial profile for a continuously flared disk is predicted to be $\propto r^{-2}$ to r^{-3} (Whitney & Hartmann 1992; Inoue et al. 2008). In our sample, however, such non-structured, azimuthally symmetric disk models are only applicable for the disk around HD 169142, and even for this star, Grady et al. (2007) pointed out that the surface brightness was explained by the inner disk flatter than the outer one or with an inner hole. The steep slope for HD 150193 implies grain growth and settling in the outer disk. The surface brightness for the outer disk of HD 142527 declines quite steeply ($r^{-6.6}$ in the southwest, $r^{-8.9}$ in the northeast direction), which does not reconcile with disk models that are continuously flared (table 5, figure 14). The mid-infrared images by Fujiwara et al. (2006) have suggested that the inner rim of the inclined disk was directly seen, and thus the presence of a vertically thick inner wall can be responsible for the scattered light luminosity without an outer flared surface. In this way, the detection of scattered light indicates that the disk should be able to intercept the stellar light, and this does not necessarily require the classical view of a flared disk. In other words, it is suggested that the observed disks are unlikely to be young flared disks with small grains well mixed with gas, but rather evolved ones, as described in sub-subsection 5.5.7.

In order to see if our observations were sensitive to continuously flared disks, simple Monte Carlo modeling (Lucas et al. 2004) was attempted. Assuming that the dominant source of gravity is the central star and the disk is in vertical hydrostatic equilibrium (Shakura & Sunyaev 1973), the disk density ρ is expressed as $\rho(r, z) = \rho_0(r/r_0)^{-\alpha}\exp[-0.5(z/h)^2]$, where $h(r)$ is the disk scale height given by $h(r) = h_0(r/r_0)^{\beta}$. The surface density, Σ, obtained by integration along the z direction, has a radial power-law distribution, $\Sigma \propto r^{\beta-\alpha}$. In a steady accretion disk, $\Sigma \propto r^{-0.75}$ is theoretically expected and α and β should be related as $\alpha = 3(\beta - 1/2)$ (e.g., Shakura & Sunyaev 1973). Alternatively, the shallower slope of $\Sigma \propto r^{-0.5}$ deduced from the observations (Kitamura et al. 2002) can be employed. The grain albedo was assumed to be $0.3 \leq \omega \leq 0.5$ (e.g., Cotera et al. 2001). The models suggests that a highly flared disk with $\Sigma \propto r^{-0.5}$ and $\beta = 5/4$ can reproduce the relative brightness of the disk to the star for AB Aur. However, the model with $\Sigma \propto r^{-0.75}$ and $\beta = 9/8$, which is often assumed for a disk study, shows the surface brightness to be only slightly above our detection limit. Therefore, although the inferred brightness depends on many free parameters, group I sources without resolved disks, but with PAH emission, like HD 139614 and HD 179218, may be good targets for future observations with the sensitivity improved only by $\gtrsim 1$ mag arcsec^{-2} at the radii where stellar light is still dominant. Furthermore, Panić and Hogerheijde (2009) argued that a significant fraction of disks around Herbig Ae stars may have relatively small radii, suggesting that the higher contrast is the key. An additional magnitude of the contrast can be achieved using coronagraphic polarimetry. Such future observations will tell us when and how disk settlement occurs and how (inner) disk dispersal proceeds.

6. Summary

H-band ($\lambda = 1.65\,\mu$m) imaging observations were conducted with adaptive optics and an infrared coronagraph. Sixteen Herbig Ae/Be stars and additional four Vega-like stars were observed. In our observations, a spatial resolution of 0.″1 was achieved on average, and we obtained a contrast of 10^5 at 1″, owing to the use of the coronagraph and PSF-subtraction.

1. Circumstellar disks were resolved around 5 out of 15 Herbig Ae stars (1–10 Myr) from $r = \sim$60–230 AU out to a few to several 100 AU. Our imaging observations revealed disks with various morphologies, which had never been predicted from the SEDs. The disks were detected in the brightness range from about 10 mag arcsec^{-2} down to 18 mag arcsec^{-2}.
2. The maximum fractional luminosity in scattered light ($L_{\rm scat}/L_{\rm total}$) for optically thick disks is on the order of 10^{-2}, whereas that for optically thin disks is a few $\times 10^{-3}$.
3. The detection rate in scattered light seems to be correlated with a prediction of disk flaring from the SED; the predicted flared disks tend to be detected in scattered light. However, the revealed disk structure and the inner disk property known from other observations imply that the resolved disks in scattered light are rather evolved. The resolved structures suggest that the disks are not continuously flared.
4. The disk brightness does not show a correlation with the stellar age and the circumstellar mass. Bright disks are surrounded by long-lived envelopes (AB Aur, HD 142527, HD 100546), and at the same time they are structured, showing such features as spiral arms. The diversity of the disk structure detected in the present sample could be attributed to the stellar multiplicity and the initial condition of the local star-forming environments.

We appreciate the support from the Subaru Telescope staff, especially from H. Suto, K. Murakawa, M. Ishii, S. Harasawa, M. Letawski, S. Ohya, N. Takato for making our observations successful. We are grateful to Dr. Carol Grady for her valuable comments throughout our entire study on Herbig Ae disks. MF was being supported by the JSPS Research Fellowships for Young Scientists. MT was supported by Grants-in-Aid for Scientific Research on Priority Areas, "Development of Extra-Solar Planetary Science" from the Ministry of Education, Culture, Science and Technology (16077101, 16077204). YI is supported by the Global Centers of Excellence (GCOE) Program: "Foundation of International Center for Planetary Science" from MEXT. This publication makes use of data products from the Two Micron All Sky Survey, which is a joint project of the University of Massachusetts and the Infrared Processing and Analysis Center/California Institute of Technology, funded by the National Aeronautics and Space Administration and the National Science Foundation. Data analysis was in part carried out on common use data analysis computer system at the Astronomy Data Center, ADC, of the National Astronomical Observatory of Japan.

Appendix 1. Notes on Non-Detections of Disks in Scattered Light

HD 144432 — HD 144432 is a known binary with a late-type (K4–K7) weak-line T Tauri star HD 144432 B (Pérez et al. 2004; Carmona et al. 2007). The X-ray detection of HD 144432 B also supports the fact that the companion is a T Tauri star (Stelzer et al. 2009). Stelzer et al. (2009) reported the separation of 1.″45 and the P.A. of 3.°0 by the K-band AO imaging performed in 1993–1996. Although Pérez et al. (2004) measured 1.″4 and −7° in 2002, the AO results by Stelzer et al. (2009) are more consistent with our measurement, and inconsistent with the hypothesis that HD 144432 is a background star. Our observing condition was bad with the shortest total exposure time and the largest FWHM, but a bright disk like the one around HD 142527 should have been detected if it exists.

KK Oph — KK Oph is a known binary. The separation and the P.A. (table 4) are in agreement with those derived by IR speckle observations conducted in 1992 ($\rho = 1.''61 \pm 0.''02$, P.A. $= 247.°2 \pm 0.°5$: Leinert et al. 1997), thus confirming the common proper motion of the companion to the primary star. Carmona, van den Ancker, and Henning (2007) derived the spectral type of G6Ve by their optical spectroscopy. There are many point sources in the FOV of CIAO, since KK Oph is located near the Galactic plane ($l = 357.°1, b = 7.°5$). Multi-wavelength or -epoch observations are needed to distinguish other possible young stars in this region.

HD 190073 (V1295 Aql) — The distance of HD 190073 (A2IV: Mora et al. 2001) is uncertain, and that addressed in the literature ranges from 290 pc to 5000 pc (van den Ancker et al. 1998; Vieira et al. 2003). The SED suggests that the distance attenuation for the Kurucz model atmosphere using $d = 290$ pc required the stellar radius of $\sim 3\,R_\odot$, which is not unreasonable. This implies that the actual distance is not far from 290 pc. No circumstellar material was found in our observations, although the PSF was not satisfactorily subtracted due to the highly variable seeing, and the region $r < 550$ AU was severely affected by the residual.

HD 200775 — HD 200775 is an illuminating source of NGC 7023. The reflection nebula NGC 7023 has received the attention in terms of the "unidentified IR features", and the star itself has also been well studied as a classical Herbig Ae/Be star. HD 200775 has an early spectral type, B3 (Hernández et al. 2004) and located relatively closer to us ($d = 430$ pc) than other Herbig Be stars. The biconical cavity, which is thought to be a remnant of past outflow activity, has been observed in CO and H I (Fuente et al. 1998). Their results indicate that the outflow direction is east–west, and consequently the disk elongation is likely to be in north–south. Fuente et al. (2001) failed to detect the 1.3 mm continuum emission, and derived the upper limit of the disk mass, $< 0.002\,M_\odot$. Our observations found neither a circumstellar disk nor reflection nebulosity around HD 200775. However, we would not have detected a circumstellar disk with the similar size and brightness as those of the resolved disks around several Herbig Ae stars due to the large distance of HD 200775 and our shallow exposures. Okamoto et al. (2009) has found extended emission likely to be attributed to a flared disk with ~ 1000 AU radius in mid-infrared. Thus, the object deserves future deep imaging in NIR.

MWC 480 (HD 31648) — The presence of a circumstellar disk is undoubted, since it has been resolved in millimeter observations (Mannings & Sargent 1997). The disk was resolved in both 1.3 mm dust continuum and CO line emission, giving the P.A. of the disk elongation $157° \pm 4°$. The line emission predicts the disk being extended out to about 245 AU ($\sim 1.''8$) in radius (Dent et al. 2005), but we could not find the signature of a corresponding disk in our scattered-light observations, which is in agreement with the non-detection in the deeper imaging by the HST (Augereau et al. 2001).

HD 34282 — The CO Keplerian disk has been spatially resolved, and the dust continuum emission has also been marginally resolved (Piétu et al. 2003), even though HD 34282 is somewhat distant, located at about 350 pc. The outer disk radius in millimeter observations is $R_{\rm out} \sim 2''$, which is not too small for our imaging. In addition, a flared disk predicted based on the SED suggests the high possibility of resolving the disk also in scattered light. However, no prominent structure was found in our study. A disk with $2''$ radius might be barely missed by our imaging, and would be a good target for higher-contrast imaging. The disk is likely to be in a transition phase with the evolved inner disk based on the mid-infrared SED (Acke et al. 2009).

HD 139614 — The face-on geometry was suggested from the slight variation, the small $v\sin i$ ($24\,{\rm km\,s^{-1}}$: Dunkin et al. 1997b), and the small polarization (Yudin et al. 1999). HD 139614 and HD 169142 have similar properties, such as the single-peaked Hα emission, low $v\sin i$, and abundance (Dunkin et al. 1997a). HD 139614 and HD 169142 are both classified as group I sources for which the detection in scattered light are predicted. However, while we detected a circumstellar disk around HD 169142 (sub-subsection 5.1.5), did not resolve HD 139614 even with the higher sensitivity. The reason for non-detection could be found in the difference from HD 169142, such as the weaker PAH emission (Acke & van den Ancker 2004; Meeus et al. 2001), the lower level of polarization, or a slightly shallower slope of the SED in submillimeter and millimeter range (Acke et al. 2004). Alternatively, the smaller disk size may produce non-detection. Considering that the nearly face-on disk around HD 169142 was barely detected in our observations, the non-detection around HD 139614 might be understandable. There are at least five point sources detected in the FOV of CIAO. The star is located at low galactic latitude, suggesting that the other point sources are more likely to be background objects.

HD 149914 — HD 149914 is found in the list of Herbig Ae/Be stars (Malfait et al. 1998), but it shows little NIR excess, suggesting the boundary nature between PMS and Vega-like stars. The optical polarization, $p = 2.5\%$ (Bhatt & Manoj 2000), was fairly large for a Herbig Ae/Be star in its later evolutionary phase. The star belongs to the Upper Scorpius association (de Zeeuw et al. 1999), and the distance of HD 149914 ($d = 165$ pc) was given by the Hipparcos. The relatively small distance becomes an advantage for resolving the circumstellar structure, in the transient phase from Herbig Ae/Be to Vega-like stars. Unfortunately, however, the PSF shape of the reference star was different from that of HD 149914 and no other appropriate PSFs were found in the datasets obtained in 2004 June. The residual intensity remains

circularly extended to $r \sim 2\farcs5$, which is possibly due to the PSF mismatch. The upper limit was poorly constrained for this reason, and we can only say that the bright disk with the fractional luminosity of scattered light $\sim 10^{-2}$ does not exist in the outside of $r \sim 1\farcs5$.

VV Ser — VV Ser is a UXor-type variable star (e.g., Rostopchina et al. 2001), suggesting an edge-on disk with an azimuthally inhomogeneous structure. Leinert et al. (2001) carried out the NIR speckle observations and resolved it along the east–west direction with the FWHM of $\sim 0\farcs6 \pm 0\farcs2$. Polarization measurements showed a polarization position angle of 70°–90° (Oudmaijer et al. 2001; Rostopchina et al. 2001). Those previous observations suggest that there is a high possibility to resolve the edge-on disk, despite its relatively large distance. The resultant image after the PSF-subtraction, however, shows no circumstellar emission. Pontoppidan et al. (2007) reported the Spitzer finding of large scale nebulosity due to transiently heated grains. They interpreted the dark wedge seen in the Spitzer image as being a shadow of a central disk blocking UV photons. The disk radius they used in the paper ($\sim$50 AU) is not inconsistent with our results.

We detected many point sources in this field, with 22 stars ranging from $H = 13.9$ mag to 21.1 mag. The brightest one at the separation of $7\farcs39$ has been reported in Li et al. (1994) and Testi, Palla, and Natta (1998), but deeper imaging and the PSF-subtraction enabled us to find fainter sources closer to VV Ser. The closest one, named VV Ser B in table 4, has a separation of $2\farcs541 \pm 0\farcs006$, and this is a candidate of a companion star due to its proximity. Testi, Palla, and Natta (1998) found the density enhancement of sources around VV Ser by the wide field ($r \sim 200''$) imaging. Our observations show no concentration toward VV Ser in this small FOV.

HD 176386 — HD 176386 is located in the Corona Australis molecular cloud. There exists another Herbig Ae/Be star TY CrA at about 55″ northeast of HD 176386, and these two stars share a common proper motion. The prominent optical nebulosity surrounds TY CrA and HD 176386. The slight IR excess (Bibo et al. 1992) and the accretion activity in the intermediate phase between other Herbig Ae/Be stars and β Pic (Grady et al. 1993) indicate that HD 176386 is in a late evolutionary stage. Our observations could not detect a circumstellar disk, and only faint nebulous emission was found in the northwest direction of HD 176386. Although the companion star is saturated in our images, its position was safely measured while taking a slightly large aperture for the centroid measurement (20 pixels in radius), and given in table 4.

HD 179218 — HD 179218 has several signs of the presence of a flared disk, such as the strong PAH emission and the similar behavior to AB Aur and HD 100546 in the millimeter SED and IR spectra (Acke & van den Ancker 2004). However, we could not find the extended circumstellar disk. The disadvantage for the imaging of HD 179218 is its distance, $d = 240^{+70}_{-40}$ pc (van den Ancker et al. 1998). Assuming the same disk as detected around HD 100546 (Augereau et al. 2001), the surface brightness drops below 16 mag arcsec^{-2} at $r > 250$ AU, which could not have been detected in our observations. If the disk has the same brightness as that of AB Aur, we would have detected it. In addition, the angular size of the disk is predicted to be less than 1″ (Dent et al. 2005; Panić & Hogerheijde 2009). Moreover, Harker et al. (2005) reported that the vertical height of the dust disk is 4-times smaller than that of HD 100546 and than those expected for optically thick disks without dust settling. The less flaring might result in the non-detection.

There are 63 sources found in the brightness range of $H = 11.9$ mag to 20.0 mag. Since HD 179218 is close to the Galactic plane ($\ell = 49\fdg2$, $b = 2\fdg9$), most sources are likely to be background objects. We listed the close and bright source in table 4, as HD 179218 B with a separation of $2\farcs539 \pm 0\farcs006$. Even if HD 179218 B is a companion star, it might contribute little to reduce the size of the disk around HD 179218 due to the relatively wide projected separation of 609 AU.

HD 131885 — HD 131885 has been classified as a Vega-like star (Mannings & Barlow 1998) with a large IR excess, $L_{\rm IR}/L_* = 1.8 \times 10^{-3}$ (Bhatt & Manoj 2000). Bhatt and Manoj (2000) obtained the large polarization as a Vega-like star, $p = 0.57 \pm 0.07\%$. We found another point source near HD 131885, with a separation and P.A. of $2\farcs19$ and $284\fdg5$, respectively. This source can be a companion star based on its proximity. The brightness of the companion was not measured because it was completely saturated in a 5 s exposure. The rough estimate of the brightness ratio was obtained from the ratio of halo intensity between the primary and the companion star. The PSF of the companion was satisfactory subtracted when using the ratio of $\Delta H \sim 2.6$ mag. Note that if the occulting mask effectively reduced the halo of the primary star, the brightness ratio should be larger.

HD 184761 — HD 184761 was identified as a Vega-like star by Miroshnichenko et al. (1999). The star has little NIR excess, does not show the emission lines, and located on ZAMS in the H–R diagram. Miroshnichenko et al. (1999) also reported that the amount of FIR excess was comparable to that of β Pic. Our results show no significant circumstellar material around HD 184761. Our H-band images suggest the possible tenuous nebulosity between HD 184761 and the star in the east. Following Kalas et al. (2002), the comparison was attempted between the position of HD 184761 ($\ell = 61\fdg9$, $b = 3\farcs4$) and the Na I absorption contours by Sfeir et al. (1999), which is an indicator of the interstellar gas density. In the direction of HD 184761, the boundary of Local Bubble is located at less than 50 pc, suggesting that the cirrus emission may contribute to the FIR excess of HD 184761 in spite of the distance smaller than 100 pc. However, while the reflection nebulosities around three sources among six in Kalas et al. (2002) are also found in the archive images of the DSS, the DSS does not indicate nebulosity around HD 184761. The similar resolution imaging as that carried out by Kalas et al. (2002) will be useful to confirm the cirrus contribution to the IR excess. If the excess is circumstellar, the fitted black body with $T = 370$ K suggests that the debris cloud exists closer to the star than most Vega-like stars showing the excess emission peaked in FIR.

We note that the H-band brightness ($H = 5.52$) tabulated in Miroshnichenko et al. (1999) could be too bright, or the star is variable. In our observations, a 10 s exposure for $H = 5.5$ star should result in saturation of the halo widely outside the mask. Therefore, $H = 6.13$ in the 2MASS catalog seems to be more reasonable, and we adopted $H = 6.1$ in this work.

HD 191089 — HD 191089 is a nearby Vega-like star

(Mannings & Barlow 1998) with a large IR excess ($L_{\rm IR}/L_* = 1.3 \times 10^{-3}$: Zuckerman & Song 2004). Its age has been estimated to be < 100 Myr by several methods (Zuckerman & Song 2004). It is likely that the IR excess is intrinsic, not the interstellar cirrus origin, since it is located in the Local Bubble (Kalas et al. 2002). The PSF-subtracted image shows no circumstellar structure, although the residual emission was slightly extended northern direction for both epoch datasets taken on June 4 and 6. Since the residual pattern was varied with time, we concluded the residual emission was not real. Even if the emission is a real structure, it is expected to be faint, and to appear in the vicinity of the star. Therefore, careful deep imaging is required under a good seeing condition or in space to obtain disk imagery.

HD 218396 — HD 218396 has been identified as a debris disk source (e.g., Sylvester et al. 1996). Although the IR excess is not so large ($L_{\rm IR}/L_* = 2.0 \times 10^{-4}$), the star is nearby ($d = 39.4$ pc: van Leeuwen 2007), which is an advantage for direct imaging. In addition, its age is estimated to be 30–160 Myr (e.g., Zuckerman & Song 2004), indicating that it is a young MS star. Our imaging was too shallow to detect a debris disk fainter than 16.0 mag arcsec^{-2} (at $r > 2\farcs5$), but a bright asymmetric structure like the edge-on disk of β Pic would have been found if it exists (Mouillet et al. 1997). The system has received considerable attention, since the discovery of three planets (Marois et al. 2008). The most distant planet was also detected at $1\farcs7$ from the star, revealing after data reductions optimized to point-source detection (Fukagawa et al. 2009).

References

Acke, B., Min, M., van den Ancker, M. E., Bouwman, J., Ochsendorf, B., Juhasz, A., & Waters, L. B. F. M. 2009, A&A, 502, L17
Acke, B., & van den Ancker, M. E. 2004, A&A, 426, 151
Acke, B., van den Ancker, M. E., Dullemond, C. P., van Boekel, R., & Waters, L. B. F. M. 2004, A&A, 422, 621
Adams, F. C., Lada, C. J., & Shu, F. H. 1987, ApJ, 312, 788
Adams, F. C., Lada, C. J., & Shu, F. H. 1988, ApJ, 326, 865
Alecian, E., et al. 2008, MNRAS, 385, 391
Alonso-Albi, T., Fuente, A., Bachiller, R., Neri, R., Planesas, P., Testi, L., Berné, O., & Joblin, C. 2009, A&A, 497, 117
Ardila, D. R., Golimowski, D. A., Krist, J. E., Clampin, M., Ford, H. C., & Illingworth, G. D. 2007, ApJ, 665, 512
Augereau, J. C., Lagrange, A. M., Mouillet, D., & Ménard, F. 1999, A&A, 350, L51
Augereau, J. C., Lagrange, A. M., Mouillet, D., & Ménard, F. 2001, A&A, 365, 78
Bastien, P., & Ménard, F. 1988, ApJ, 326, 334
Bessel, M. S., Castelli, F., & Plez, B. 1998, A&A, 333, 231
Bhatt, H. C., & Manoj, P. 2000, A&A, 362, 978
Bibo, E. A., Thé, P. S., & Dawanas, D. N. 1992, A&A, 260, 293
Bouwman, J., de Koter, A., van den Ancker, M. E., & Waters, L. B. F. M. 2000, A&A, 360, 213
Burrows, C. J., et al. 1996, ApJ, 473, 437
Calvet, N., D'Alessio, P., Hartmann, L., Wilner, D., Walsh, A., & Sitko, M. 2002, ApJ, 568, 1008
Carmona, A., van den Ancker, M. E., & Henning, Th. 2007, A&A, 464, 687
Chiang, E. I., & Goldreich, P. 1997, ApJ, 490, 368
Chiang, E. I., Joung, M. K., Creech-Eakman, M. J., Qi, C., Kessler, J. E., Blake, G. A., & van Dishoeck, E. F. 2001, ApJ, 547, 1077
Clampin, M., et al. 2003, AJ, 126, 385
Cohen, M., Emerson, J. P., & Beichman, C. A. 1989, ApJ, 339, 455
Collins, K. A., et al. 2009, ApJ, 697, 557
Cotera, A. S., et al. 2001, ApJ, 556, 958
de Lara, E., Chavarria-K, C., & López-Molina, G. 1991, A&A, 243, 139
de Zeeuw, P. T., Hoogerwerf, R., de Bruijne, J. H. J., Brown, A. G. A., & Blaauw, A. 1999, AJ, 117, 354
Debes, J. H., Weinberger, A. J., & Schneider, G. 2008, ApJ, 673, L191
Dent, W. R. F., Greaves, J. S., & Coulson, I. M. 2005, MNRAS, 359, 663
Devine, D., Grady, C. A., Kimble, R. A., Woodgate, B., Bruhweiler, F. C., Boggess, A., Linsky, J. L., & Clampin, M. 2000, ApJ, 542, L115
Doering, R. L., Meixner, M., Holfeltz, S. T., Krist, J. E., Ardila, D. R., Kamp, I., Clampin, M. C., & Lubow, S. H. 2007, AJ, 133, 2122
Dullemond, C. P., Dominik, C., & Natta, A. 2001, ApJ, 560, 957
Dullemond, C. P., van den Ancker, M. E., Acke, B., & van Boekel, R. 2003, ApJ, 594, L47
Dunkin, S. K., Barlow, M. J., & Ryan, S. G. 1997a, MNRAS, 286, 604
Dunkin, S. K., Barlow, M. J., & Ryan, S. G. 1997b, MNRAS, 290, 165
Dutrey, A., Guilloteau, S., & Simon, M. 1994, A&A, 286, 149
Eisner, J. A., Lane, B. F., Hillenbrand, L. A., Akeson, R. L., & Sargent, A. I. 2004, ApJ, 613, 1049
Elsässer, H., & Staude, H. J. 1978, A&A, 70, L3
Fuente, A., Martín-Pintado, J., Rodríguez-Franco, A., & Moriarty-Schieven, G. D. 1998, A&A, 339, 575
Fuente, A., Neri, R., Martin-Pintado, J., Bachiller, R., Rodriguez-Franco, A., & Palla, F. 2001, A&A, 366, 873
Fujiwara, H., et al. 2006, ApJ, 644, L133
Fukagawa, M., et al. 2004, ApJ, 605, L53
Fukagawa, M., Itoh, Y., Tamura, M., Oasa, Y., Hayashi, S. S., Fujita, Y., Shibai, H., & Hayashi, M. 2009, ApJ, 696, L1
Fukagawa, M., Tamura, M., Itoh, Y., Hayashi, S. S., & Oasa, Y. 2003, ApJ, 590, L49
Fukagawa, M., Tamura, M., Itoh, Y., Kudo, T., Imaeda, Y., Oasa, Y., Hayashi, S. S., & Hayashi, M. 2006, ApJ, 636, L153
Garcia Lopez, R., Natta, A., Testi, L., & Habart, E. 2006, A&A, 459, 837
Grady, C. A., et al. 2000, ApJ, 544, 895
Grady, C. A., et al. 2001, AJ, 122, 3396
Grady, C. A., et al. 2004, ApJ, 608, 809
Grady, C. A., et al. 2005b, ApJ, 630, 958
Grady, C. A., et al. 2007, ApJ, 665, 1391
Grady, C. A., et al. 2009, ApJ, 699, 1822
Grady, C. A., Pérez, M. R., & Thé, P. S. 1993, A&A, 274, 847
Grady, C. A., Woodgate, B., Heap, S. R., Bowers, C., Nuth, J. A., III, Herczeg, G. J., & Hill, H. G. M. 2005a, ApJ, 620, 470
Greaves, J. S., Mannings, V., & Holland, W. S. 2000, Icarus, 143, 155
Guilloteau, S., Dutrey, A., & Simon, M. 1999, A&A, 348, 570

Habart, E., Natta, A., & Krügel, E. 2004, A&A, 427, 179
Harker, D. E., Woodward, C. E., Wooden, D. H., & Temi, P. 2005, ApJ, 622, 430
Hartmann, L., Kenyon, S. J., & Calvet, N. 1993, ApJ, 407, 219
Herbig, G. H. 1960, ApJS, 4, 337
Hernández, J., Calvet, N., Briceño, C., Hartmann, L., & Berlind, P. 2004, AJ, 127, 1682
Houk, N. 1978, Michigan Catalogue of Two-Dimensional Spectral Types for the HD Stars, Vol.1 (Ann Arbor: Department of Astronomy, University of Michigan)
Houk, N. 1982, Michigan Catalogue of Two-Dimensional Spectral Types for the HD Stars, Vol.3 (Ann Arbor: Department of Astronomy, University of Michigan)
Houk, N., & Smith-Moore, M. 1988, Michigan Catalogue of Two-Dimensional Spectral Types for the HD Stars, Vol.4 (Ann Arbor: Department of Astronomy, University of Michigan)
Inoue, A. K., Honda, M., Nakamoto, T., & Oka, A. 2008, PASJ, 60, 557
Isella, A., Testi, L., Natta, A., Neri, R., Wilner, D., & Qi, C. 2007, A&A, 469, 213
Itoh, Y., et al. 2002, PASJ, 54, 963
Itoh, Y., et al. 2005, ApJ, 620, 984
Iye, M., et al. 2004, PASJ, 56, 381
Kalas, P., Fitzgerald, M. P., & Graham, J. R. 2007, ApJ, 661, L85
Kalas, P., Graham, J. R., Beckwith, S. V. W., Jewitt, D. C., & Lloyd, J. P. 2002, ApJ, 567, 999
Keller, L. D., et al. 2008, ApJ, 684, 411
Kenyon, S. J., & Bromley, B. C. 2004, AJ, 127, 513
Kitamura, Y., Momose, M., Yokogawa, S., Kawabe, R., Tamura, M., & Ida, S. 2002, ApJ, 581, 357
Köhler, M., Mann, I., & Li, A. 2008, ApJ, 686, L95
Krist, J. E., Stapelfeldt, K. R., Ménard, F., Padgett, D. L., & Burrows, C. J. 2000, ApJ, 538, 793
Kuhn, J. R., Potter, D., & Parise, B. 2001, ApJ, 553, L189
Lachaume, R., Dominik, C., Lanz, T., & Habing, H. J. 1999, A&A, 348, 897
Leinert, Ch., et al. 2004, A&A, 423, 537
Leinert, Ch., Haas, M., Ábrahám, P., & Richichi, A. 2001, A&A, 375, 927
Leinert, C., Richichi, A., & Haas, M. 1997, A&A, 318, 472
Li, W., Evans, N.J., II, Harvey, P. M., & Colomé, C. 1994, ApJ, 433, 199
Lucas, P. W., et al. 2004, MNRAS, 352, 1347
Lyot, M. B. 1939, MNRAS, 99, 580
Malfait, K., Bogaert, E., & Waelkens, C. 1998, A&A, 331, 211
Mannings, V., & Barlow, M. J. 1998, ApJ, 497, 330
Mannings, V., & Sargent, A. I. 1997, ApJ, 490, 792
Mannings, V., & Sargent, A. I. 2000, ApJ, 529, 391
Manoj, P., Bhatt, H. C., Maheswar, G., & Muneer, S. 2006, ApJ, 653, 657
Marois, C., Macintosh, B., Barman, T., Zuckerman, B., Song, I., Patience, J., Lafrenière, D., & Doyon, R. 2008, Science, 322, 1348
McCabe, C., Duchêne, G., & Ghez, A. M. 2002, ApJ, 575, 974
McCaughrean, M. J., & O'Dell, C. R. 1996, AJ, 111, 1977
Meeus, G., Waters, L. B. F. M., Bouwman, J., van den Ancker, M. E., Waelkens, C., & Malfait, K. 2001, A&A, 365, 476
Merín, B., et al. 2004, A&A, 419, 301
Miroshnichenko, A. S., Christopher, L. M., Bjorkman, K. S., Morrison, N. D., Kuratov, K. S., & Wisniewski, J. P. 1999, MNRAS, 302, 612
Miyake, K., & Nakagawa, Y. 1993, Icarus, 106, 20
Monet, D. G., et al. 2003, AJ, 125, 984
Mora, A., et al. 2001, A&A, 378, 116
Mouillet, D., Lagrange, A.-M., Beuzit, J.-L., & Renaud, N. 1997, A&A, 324, 1083
Mundt, R., & Fried, J. W. 1983, ApJ, 274, L83
Natta, A., Prusti, T., Neri, R., Wooden, D., Grinin, V. P., & Mannings, V. 2001, A&A, 371, 186
O'Dell, C. R., Wen, Z., & Hu, X. 1993, ApJ, 410, 696
Ohashi, N. et al. 2010, ApJ submitted
Okamoto, Y. K., et al. 2009, ApJ, 706, 665
Oppenheimer, B. R., et al. 2008, ApJ, 679, 1574
Oudmaijer, R. D., et al. 2001, A&A, 379, 564
Palla, F., & Stahler, S. W. 1999, ApJ, 525, 772
Panić, O., & Hogerheijde, M. R. 2009, A&A, 508, 707
Panić, O., Hogerheijde, M. R., Wilner, D., & Qi, C. 2008, A&A, 491, 219
Pérez, M. R., van den Ancker, M. E., de Winter, D., & Bopp, B. W. 2004, A&A, 416, 647
Perrin, M. D., Schneider, G., Duchene, G., Pinte, C., Grady, C. A., Wisniewski, J. P., & Hines, D. C. 2009, ApJ, 707, L132
Pezzuto, S., Strafella, F., & Lorenzetti, D. 1997, ApJ, 485, 290
Piétu, V., Dutrey, A., & Kahane, C. 2003, A&A, 398, 565
Piétu, V., Guilloteau, S., & Dutrey, A. 2005, A&A, 443, 945
Pirzkal, N., Spillar, E. J., & Dyck, H. M. 1997, ApJ, 481, 392
Pontoppidan, K. M., Dullemond, C. P., Blake, G. A., Evans, N. J., II, Geers, V. C., Harvey, P. M., & Spiesman, W. 2007, ApJ, 656, 991
Raman, A., Lisanti, M., Wilner, D. J., Qi, C., & Hogerheijde, M. 2006, AJ, 131, 2290
Rostopchina, A. N., Grinin, V. P., & Shakhovskoi, D. N. 2001, Astron. Lett., 27, 39
Sartori, M. J., Lépine, J. R. D., & Dias, W. S. 2003, A&A, 404, 913
Schneider, G., et al. 1999, ApJ, 513, L127
Schneider, G., et al. 2006, ApJ, 650, 414
Schneider, G., Silverstone, M. D., & Hines, D. C. 2005, ApJ, 629, L117
Schneider, G., Wood, K., Silverstone, M. D., Hines, D. C., Koerner, D. W., Whitney, B. A., Bjorkman, J. E., & Lowrance, P. J. 2003, AJ, 125, 1467
Sfeir, D. M., Lallement, R., Crifo, F., & Welsh, B. Y. 1999, A&A, 346, 785
Shakura, N. I., & Sunyaev, R. A. 1973, A&A, 24, 337
Simon, M., Dutrey, A., & Guilloteau, S. 2001, ApJ, 545, 1034
Sitko, M. L., et al. 2008, ApJ, 678, 1070
Skiff, B. A. 2003, Catalogue of Stellar Spectral Classifications (Flagstaff, AZ: Lowell Observatory)
Stapelfeldt, K. R., Krist, J. E., Ménard, F., Bouvier, J., Padgett, D. L., & Burrows, C. J. 1998, ApJ, 502, L65
Stelzer, B., Micela, G., Hamaguchi, K., & Schmitt, J. H. M. M. 2006, A&A, 457, 223
Stelzer, B., Robrade, J., Schmitt, J. H. M. M., & Bouvier, J. 2009, A&A, 493, 1109
Strom, K. M., Newton, G., Strom, S. E., Seaman, R. L., Carrasco, L., Cruz-Gonzalez, I., Serrano, A., & Grasdalen, G. L. 1989, ApJS, 71, 183
Sylvester, R. J., Dunkin, S. K., & Barlow, M. J. 2001, MNRAS, 327, 133
Sylvester, R. J., Skinner, C. J., Barlow, M. J., & Mannings, V. 1996, MNRAS, 279, 915
Takami, H., et al. 2004, PASJ, 56, 225
Tamura, M., et al. 2000, Proc. SPIE, 4008, 1153
Teixeira, R., Ducourant, C., Sartori, M. J., Camargo, J. I. B., Périé, J. P., Lépine, J. R. D., & Benevides-Soares, P. 2000, A&A, 361, 1143
Testi, L., Palla, F., & Natta, A. 1998, A&AS, 133, 81

van Boekel, R., Waters, L. B. F. M., Dominik, C., Bouwman, J., de Koter, A., Dullemond, C. P., & Paresce, F. 2003, A&A, 400, L21
van den Ancker, M. E., Bouwman, J., Wesselius, P. R., Waters, L. B. F. M., Dougherty, S. M., & van Dishoeck, E. F. 2000, A&A, 357, 325
van den Ancker, M. E., de Winter, D., & Tjin A Djie, H. R. E. 1998, A&A, 330, 145
van den Ancker, M. E., Thé, P. S., Tjin A Djie, H. R. E., Catala, C., de Winter, D., Blondel, P. F. C., & Waters, L. B. F. M. 1997, A&A, 324, L33
van Leeuwen, F. 2007, A&A, 474, 653
Verhoeff, A. 2009, PhD Thesis, University of Amsterdam
Vieira, S. L. A., Corradi, W. J. B., Alencar, S. H. P., Mendes, L. T. S., Torres, C. A. O., Quast, G. R., Guimarães, M. M., & da Silva, L. 2003, AJ, 126, 2971
Vieira, S. L. A., Pogodin, M. A., & Franco, G. A. P. 1999, A&A, 345, 559
Vink, J. S., Drew, J. E., Harries, T. J., & Oudmaijer, R. D. 2002, MNRAS, 337, 356
Webb, R. A., Zuckerman, B., Platais, I., Patience, J., White, R. J., Schwartz, M. J., & McCarthy, C. 1999, ApJ, 512, L63
Weinberger, A. J., et al. 2002, ApJ, 566, 409
Weinberger, A. J., Becklin, E. E., Schneider, G., Smith, B. A., Lowrance, P. J., Silverstone, M. D., Zuckerman, B., & Terrile, R. J. 1999, ApJ, 525, L53
White, R. J., Ghez, A. M., Reid, I. N., & Schultz, G. 1999, ApJ, 520, 811
Whitney, B. A., & Hartmann, L. 1992, ApJ, 395, 529
Wisniewski, J. P., Clampin, M., Grady, C. A., Ardila, D. R., Ford, H. C., Golimowski, D. A., Illingworth, G. D., & Krist, J. E. 2008, ApJ, 682, 548
Yudin, R. V., Clarke, D., & Smith, R. A. 1999, A&A, 345, 547
Zuckerman, B., & Song, I. 2004, ApJ, 603, 738